A STUDY OF A RIGID FRAME HIGHWAY BRIDGE IN VIRGINIA

by

H. L. Kinnier and F. W. Barton
Faculty Research Engineers
University of Virginia

Virginia Highway & Transportation Research Council
(A Cooperative Organization Sponsored Jointly by the Virginia
Department of Highways & Transportation and the University of Virginia)

Charlottesville, Virginia

April 1975
VHTRC 75-R47

ABSTRACT

This report describes the experimental and analytical study of a rigid frame highway bridge conducted under the auspices of the Federal Highway Administration and the Virginia Highway & Transportation Research Council. Data collected during the experimental phase provided measures of strains and deflections at midspan of selected girders and strain data in the vicinity of one of the haunches. These data, along with calculated values of bending moment based on the measurements, provided a basis for evaluating the design and for comparison with subsequently calculated analytical data.

The theoretical study was performed by modeling a typical rigid frame girder as a series of flexural elements and analyzing the model using a finite element computer program. Results obtained included shears, moments and deflections at each node point on the model; also influence lines for moment and deflection at midspan and at the haunch extremities were generated. Calculated values of moment and deflection were found to compare quite favorably with those determined from the experimental study. Effects of various parameters on moments and deflections were studied by varying such characteristics as haunch representation, support conditions and member representation. Variations in support conditions were found to be the only parameter to have any significant effect on moments and deflections, and then primarily on stresses in the vicinity in the haunch.

A STUDY OF A RIGID FRAME HIGHWAY BRIDGE IN VIRGINIA

by

H. L. Kinnier and F. W. Barton
Faculty Research Engineers
University of Virginia

1. INTRODUCTION

1.1 Problem Statement

There are many areas of structural design in which completely rational procedures either are not feasible or require so many simplifying assumptions that the final formulations render results that are somewhat questionable. In such cases design engineers rely on sound judgment, intuition, and experience, in addition to calculations. In many instances, when the problem is common enough, standard rules of design are developed, adjusted, and modified as the finished structure is observed and studied through its service life.

In the stress analysis and structural design of a rigid frame, which is now being widely used in highway bridges, certain idealizing assumptions are made so that a reasonably uncomplicated solution can be effected. Several of the assumptions concern the effective lengths of the members and the effects of the variation in depths of the haunches at the ends of the members. It appears worthwhile to evaluate these assumptions by comparing theoretical results based on these simplifications with measured experimental data from the same type of structure.

1.2 Objective

The purpose of this research project was to compare the live load design stresses and influence diagrams theoretically calculated on the basis of several commonly used assumptions with the stresses and deflections determined experimentally during the controlled loading of an in-use rigid frame highway bridge. More specifically, the objectives of this study divide into two general areas briefly described as follows:

1. To determine the resulting strains and deflections at selected points of a rigid frame highway bridge due to the passage of a test vehicle simulating a standard highway bridge loading moving at speeds varying from creep up to 50 miles per hour (26.8 m/s) at selected intervals. The experimental measurements for the runs at creep speeds are reported herein. The strain and deflection measurements for the higher speeds are being studied and will be reported on by the Federal Highway Administration at a later date.

2. To compare the field measurements of strain and deflection from creep speeds of the test vehicle with currently accepted bridge design procedures, assumptions, and findings of recent research studies. In particular, efforts were made to determine the lateral distribution of the live load at midspan to the five rigid frames of the bridge and to determine the effects of various assumptions including several modelings of the haunch on influence diagrams for moment at several critical positions of an interior frame.

2. EXPERIMENTAL PROGRAM

2.1 Description of Test Structure

The test structure carries the westbound lane of Interstate Route 64 over Route 250 about three miles (4.8 km) east of Charlottesville, Virginia. The bridge and an identical structure on the eastbound lane are the first of their kind in Virginia, but it is generally felt that this design will be used more frequently where suitable because of its aesthetic value and safety features. The design has received considerable attention through a brochure circulated nationally by the Bethelehem Steel Corporation.

There are three primary attributes of this basic design; namely: (1) its considerable aesthetic value by virtue of its slender lines, its arch-like appearance, and its wide clear span, (2) the benefits from economy of material because of the continuity between the members in the individual frames, and (3) the safety benefits by virtue of the two intermediate supports of the bridge span being inclined away from the lower roadway pavement and the ordinarily used center pier being eliminated altogether. These design features conform with AASHTO safety criteria for clearance between the traveled roadway and fixed objects at roadside and were influential in the selection of this particular design.

The bridge, shown in Figures 1 and 2,* is 216 ft. (65.83 m) long and consists of five three-span welded rigid frames. The two interior supports are inclined I-shaped columns framed integrally with the welded haunched girders and supported on concrete footings with anchor bolts attached to the web in such a manner as to allow free rotation. The ends of the bridge are simply supported on shelf abutments with allowance for longitudinal movements. The structures, whose dimensions are shown in Figure 1, were designed for an HS-20-44 live load using A-36 structural steel in accordance with AASHTO Specifications, 1965. Construction was completed in late 1969 and testing took place in September 1972.

---

* All figures and tables are appended.

2.2 Test Procedure

The test vehicle was a three-axle diesel tractor semitrailer loaded to simulate an HS20-44 loading. A photograph of the truck is shown in Figure 3 and sketches giving wheel loadings and dimensions between wheels and axles are shown in Figure 4.

A total of 35 test runs were made as shown in Table 1. Ten crossings of the test vehicle were made at crawl speeds (3-5 mph) (1.3-2.2 m/s), with two runs in each of the five lanes indicated in Figure 5. One crossing was made in each of the five lanes for speeds of 15, 30, 40, 50 and 60 mph (6.7, 8.9, 17.9, 22.4, and 26.8 m/s) for an additional 25 runs. The lane positions were selected as follows:

1. Lane 1 is centered over the instrumented Frame 2.
2. Lane 2 is located to have a line of wheels directly over the instrumented Frame 2.
3. Lane 3 is centered in the right-hand traffic lane.
4. Lane 4 is centered over the middle Frame 3. A cross section of the structure is symmetrical about a vertical line through Frame 3.
5. Lane 5 is centered over Frame 4.

Both the five traffic lanes and the five structural frames are numbered from 1 to 5 in order beginning on the north side of the structure (toward Charlottesville on U. S. Route 250).

All runs were made in the westbound direction. Normal traffic, which varied from light to moderate, was not interrupted during the test period. The operator of the test vehicle would wait until traffic ahead had cleared the bridge and no traffic was in sight to the rear before beginning a test run. On occasion, 10 to 15 minute delays were required for this favorable condition. However, the entire series of tests were completed in a total of 8 hours in an afternoon and the following morning, September 6 and 7, 1972.

2.3 Instrumentation

The Federal Highway Administration furnished the instrumentation, directed its installation, and operated the equipment for the testing. The instrumentation system consisted of 64 channels of Universal signal conditioners, DC amplifiers, and recorders. By means of a patch panel the output from each amplifier was split for recording on oscillograph tapes as well as analog tapes. For this test, 45 analog type channels were available and 64 oscillogram channels were used.

SR-4 wire strain gages were placed at 29 positions and rosette gages at 8 positions on the westbound bridge as shown in Figures 6 and 7. Coordinates of haunch gages are given in Table 2. In addition, deflection gages were installed at midspan of the five frames and are also indicated in Figure 7. The deflection gages consisted of 12 in. (0.30 m) aluminum strips with one end clamped to the lower flange of the steel frames and the other end anchored in a deflected position to the ground. An SR-4 strain gage attached to the clamped end of the cantilevered strip was used to produce deflection signals which were recorded on the oscillograph trace. Figure 8 is a photograph of a typical deflection gage.

Pneumatic traffic tubes were installed on the approach roadway 50 ft. (15.2 m) ahead of the east abutment and also at a position 75 ft. (22.9 m) beyond the west abutment (see Figure 9). The recorded signals from these two pneumatic tubes provided a means of locating the test vehicle during the interval of testing and relating its position to the resulting stresses and deflections. Also, the elapsed time between the pneumatic tube signals allowed the calculation of the average speed of the test vehicle as it crossed the bridge.

Principal stresses from live loading were calculated based on data obtained from the eight strain rosettes mounted on the web of the haunch as indicated in Figure 6. The orientations of the rosettes are indicated on the sketch and it may be observed that rosette numbers 1, 2, 6, and 7 were oriented such that the clockwise gage was horizontal while all of the other rosettes were oriented such that their clockwise gage would be aligned with, or normal to, one of the stiffeners or with the centerline axis of the inclined leg.

The strain readings from the deflection gages were reduced to deflections in inches by a calibration curve for each gage which had been previously determined in the laboratories of the Federal Highway Administration.

2.4 Results

The output of the 29 SR-1 and 8 rosette strain gages, the 5 deflection gages and the 2 pneumatic tube signals was recorded as continuous traces on oscillograph tapes. Measured strains were converted to stresses from the characteristics of the gages and an assumed modulus of elasticity of 30,000,000 psi (20.7×10^{10} Pa). In addition, the output of 39 of the strain gages was recorded on analog tape, digitized, converted to strain and recorded on printout sheets after the completion of the field tests.

Midspan stresses are reported in Tables 3 and 4 and stresses from the haunch gages are reported in Tables 5 through 7. The data from eight of the gages marked by an asterisk in Tables 5-7 were reduced from oscillograph tapes in the same manner as those from the midspan gages. The stress data from the remaining 39 haunch gages were obtained from printout sheets from the special data acquisition system described in the Instrumentation section of this report.

The flexural stresses in the five frames were very sensitive to the position of the test vehicle on the deck. Table 3 reports the percentages of total moment as distributed to the five frames as indicated by the flexural stresses. These same data are plotted in Figures 10, 11 and 12. The percentages of the total moment in the frames at a particular section reflect the shift of the test vehicle in the lanes of passage. It is also noted that the relative midspan deflections for the various paths of the test vehicle runs are closely consistent with the lane position of the test vehicle. (See Table 8)

Strain data from the rosette gages were recorded continuously during the test but principal stresses were calculated only from strains recorded in the vicinity of maximum strains. A tabulation of the maximum and minimum principal stresses for each gage is given in Table 9 along with the corresponding lane in which the vehicle was traveling and the vehicle position in terms of percent of travel measured between the air hoses. From the table it is observed that most of the maximum tensile and compressive stresses were obtained with the vehicle in Lane 1, which is directly over the instrumented girder. It may also be observed that the maximum tensile stress was approximately 1800 psi (12.41 x 10^6 Pa), while the maximum compressive stress was slightly less than 1,000 psi (6.895 x 10^6 Pa). Thus that region of the haunch in which the rosette gages were located is likely to be relatively lightly stressed. It should be noted, however, that all of the rosette gages were at least 15 in. (0.38 m) from the upper or lower flange, and hence would be expected to record a somewhat reduced stress level.

A more complete recording of principal stress data including direction of principal stress for all of the gages and all of the lane loadings is provided in Tables 10-14 of the Appendix.

While for the most part, the pattern of variation of the stresses and deflections in the five frames for the five transverse lanes is predictable and logical, there is an exception in the responses to the centerline runs (Lane 4), which are centered over Frame 3. Because of the symmetry of the structure about a vertical line through Frame 3, one would expect Frames 2 and 4 to be equally stressed and Frames 1 and 5 to be equally stressed at a lower value. However, Frames 4 and 5 were stressed more heavily than 1 and 2, respectively, by a significant amount. There is no readily discernible reason for this unbalanced distribution of stresses. One's first surmise would be that the vehicle's path on the centerline runs was by error closer to Frames 4 and 5 and away from Frames 1 and 2. However, this was not the case; the position of the vehicle on its runs followed the prescribed paths closely. The slight skew of the structure would not account for this unbalanced stress condition either, as the stresses recorded were peak stresses during the run and did not occur simultaneously. A possible explanation could be a difference in the degree of restraint at the column and/or abutment supports between the two south frames relative to the two north frames. This would develop different moments throughout the frames and result in different mid-span stresses and deflections. However, such a variation in support restraint conditions is not likely.

2.5 Transverse Distribution Factors

The designer of a composite bridge span first designs the concrete deck and then the steel girder. In the girder design, AASHTO specifications direct the engineer in the selection of the following parameters:

1. The value of "n", the ratio of E_s/E_c. See Par. 1.5.2(4), p. 58[1].
2. The effective width of the concrete slab. See Par. 1.7.98, p. 130[1]; also Par. 1.5.5, p. 56[1].
3. The transverse distribution factor to be applied to a line of wheels to estimate the percentage of live load to be supported by a single girder. See Par. 1.3.1, Table 1.3.1(B), pp. 27 and 28[1].

The value of "n" and the effective width of slab have only a small influence on the section modulus for the bottom fibers. In this structure, these values vary from a high of 1,630 in.^{3} (0.0267 m^3) to a low of 1,600 in.^{3} (0.0262 m^3). This is only a 2% variation for the several combinations of "n" and flange widths listed in Table 15. The transverse distribution factor used in determining the live load moment has a much more significant influence on the girder selection process. There has been a high number of both experimental and theoretical studies made on this subject and it is recognized that the AASHTO specifications for design for this factor are conservative for most structures. In this study, the measured maximum live load stresses in the lower flanges at midspan in the five frames for the test vehicle in Lane 3 are superimposed with the stresses at the same positions for the test vehicle in Lane 5 (see Table 16). The maximum live load stresses are less than half of the design live load stresses of 9,130 psi (62.95 x 10^6 Pa). It should be pointed out that these experimental stresses are for crawl runs (static conditions) with no dynamic effects nor impact situations.

While a number of previous studies have also indicated that the AASHTO specifications for the transverse distribution of live load to stringers are generally conservative, these specifications have been in effect for a number of years with only minor changes. In this stress study of a rigid frame bridge, the theory for predicting the transverse distribution of live load developed by Hendry and Jaeger[2] in 1956 proved to correlate closely with the experimental data. Their paper presents a general method for calculating the distribution of longitudinal moments, deflections, etc., in bridge deck systems based on the assumption that the transverse system can be replaced by a uniform medium of the same total flexural rigidity. By employing the properties of harmonics, that is, assuming the beam will take the shape of a sinusoidal deflection curve, and by calculating basic properties of the structure's transverse and longitudinal sections, Hendry and Jaeger developed a means of deriving for each harmonic the distribution coefficients to be applied to the total bending moment. Their theory is applicable to a number of superstructure types, including a composite steel beam and concrete deck such as the design used in this test structure.

The test vehicle crossed the bridge two times in each of the five different lateral positions located in Figure 5. The experimental stress distributions are plotted in Figures 10, 11, and 12 for the five paths (as computed from the experimentally measured stresses). These plottings also show the distributions as calculated from the theory of Hendry and Jaeger. The respective distribution values agree closely.

Sanders and Elleby[3] mention in the conclusions of NCHRP Report #83, "Distribution of Wheel Loads on Highway Bridges", that from the data they have studied, orthotropic plate theory is the more reliable theory for predicting distribution of wheel loads in highway bridges for beam and slab bridges. A table included in their report, which compared for a number of bridges the distribution of wheel loads from the orthotropic plate theory and harmonic analysis theory with distribution from experimental studies, showed somewhat closer agreement for the orthotropic plate theory than for Hendry and Jaeger's harmonic theory for beam and slab bridges. A comparison of the experimental data with orthotropic plate theory was not undertaken in this study.

Table 3 lists data for the distribution of wheel loads to the five frames for five lateral positions as calculated from experimental data and as developed from harmonic analysis theory.

3. ANALYTICAL RESULTS

3.1 Analysis Methods

A theoretical analysis of the rigid frame bridge was conducted to verify the experimental data collected and to provide additional stress and deflection information in regions other than midspan and haunch where experimental data were lacking. Such a theoretical analysis also provides a basis for evaluating the design procedures used and, hopefully, would also provide detailed information regarding stress distribution in the haunch region of the bridge.

The analysis was performed using a finite element computer program in which a typical frame was represented as a series of flexural elements. The total rigid frame structure was subdivided into 16 separate elements, with two elements representing each end span, four elements modeling the center span, one element for each inclined leg, and three elements to represent each haunch. A sketch of the idealized structure used in this analysis is shown in Figure 13. The flexural characteristics of the actual structure were modeled as closely as possible. The stiffness matrices were formulated to represent the flexural characteristics of each of the elements taking into account

those elements in which there was a linear variation in depth. Also, in modeling the haunch, the variation in depth and the extremely stiff nature of the central portion of the haunch were incorporated in the modeling.

The moment of inertia for each cross section was calculated based on the AASHTO specifications for composite beams to take into account the concrete deck on the top flange of the girder. The controlling effective slab width from the AASHTO specifications was 12 times its thickness. Thus, for each of the elements along the deck, a portion of the 8-in. (0.203 m) slab 96 in. (2.438 m) wide was included along with the girder in calculating the moment of inertia used in the analysis. The composite section was used in negative moment areas as well as positive moment areas inasmuch as there was no apparent cracking in the deck slab.

With regard to support conditions, each of the inclined legs was assumed to be pinned at the base and the bearings at the abutments were treated as roller supports providing no restraint against horizontal motion. The actual fabrication detail provided for the inclined legs to be attached to a base plate by two anchor bolts at mid web position and for the frame to be connected to the abutments by means of slotted plates with pins to permit expansion. Thus the assumed support conditions appear reasonable.

Based on results from the theoretical analysis, and using the assumptions previously described, influence lines for moment and deflection at midspan and moments at the haunch extremities were prepared and are presented in Figures 14-17. The maximum midspan moment resulting from a unit load was calculated to be 196.7 in.-kips (22.23×10^3 N·m) while the maximum haunch bending moments at the exterior and interior extremities were -72.6 and -124.4 in.-kips (8.20×10^3 and 14.06×10^3 N·m), respectively. The maximum midspan deflection for a unit load at midspan was 0.10 in. (2.54×10^{-3} m). See Figure 15.

Using information from these influence lines, it was possible to calculate the theoretical midspan moments and midspan deflection resulting from the actual vehicle loading. The calculated deflection at midspan, using a theoretical loading based on the measured lateral load distribution, was determined to be 0.27 in. (6.86×10^{-3} m). The experimental deflection, determined from a deflection gage mounted at midspan during the test, was measured to be 0.28 in. (7.11×10^{-3} m), indicating, at least in this single measurement, extremely close agreement. Again using the experimentally determined load distribution to determine the single girder loading, the midspan moment due to the vehicle loading was calculated to be 350 ft.-kips (0.475×10^6 N·m) while the experimentally determined bending moment at midspan was approximately 335 ft.-kips (0.454×10^6 N·m), again indicating close agreement.

As was mentioned previously, all of the results presented thus far were obtained using a theoretical model developed to represent as closely as possible the actual bridge girder. Because of the possibility of some error in the representation, a limited study was undertaken to determine what differences in critical moments and deflections would result from slight variations in some of the approximations. The three assumptions which could likely be subject to some error in representation were (a) the assumed support conditions, (b) calculation of the moment of inertia based on the AASHTO specifications, and, most importantly, (c) the representation of the haunch region of the girder.

The moment of inertia of a given cross section was determined by the portion of the adjoining slab considered to act compositely with the girder. As noted earlier, the AASHTO specifications recommend an effective width of slab equal to twelve times the slab thickness. However, during examination of the experimental data, it was determined that the neutral axis as determined from strain measurements could best be matched analytically if the effective slab width used was that recommended by AASHTO for concrete Tee-beams, namely that the effective width would be taken as twelve times the thickness of the slab plus the width of the flange (corresponding to the stem of the Tee-beam). Accordingly, theoretical calculations of controlling moments and deflections were made for both types of moment of inertia approximations. Results indicated that the differences were negligible and hence the use of the original appropriate AASHTO specifications seems justified. It thus appears questionable whether different specifications for flange width for concrete Tee-beams and composite beams are necessary.

To determine the effect of different support conditions, theoretical calculations of midspan and haunch moments and centerline deflections were determined for the case in which the deck supports were pinned to the abutments to restrict any horizontal motion. The incorporation of these different end supports for the deck had negligible effects on the midspan moments and midspan deflection as may be seen in Figures 18 and 19. However, the choice of support conditions significantly affected moments in the haunch region. Influence lines for bending moment at the two haunch extremities for the two support conditions are shown in Figures 20 and 21. As may be observed, permitting the deck to move horizontally may increase the positive moment at the interior span extremity of the haunch region by as much as 400%. Roller supports still appear to be a more reasonable assumption; however, the designer should be aware of the fact that different end conditions can result in significant moments at connections, particularly when inclined legs are used.

In developing the theoretical calculations, one of the most difficult approximations was to arrive at a realistic model of the haunch. To determine the effect of various assumptions, the results obtained by what was considered to be a rational haunch model were compared with two other approximations, one in which the haunch was modeled as unreasonably stiff, and one in which the haunch was modeled as quite flexible. The rigid model was developed assuming that each flexural member representing the haunch

had a stiffness approximately 100 times that of the end span girder. The flexible model was developed assuming that each of the haunch elements had a stiffness identical to that of its continguous girder member. As noted earlier a close approximation to the actual haunch was achieved by modeling the extremities as having finite stiffness and the interior portion of the haunch as being rigid. The precise choice of the rigid portion is somewhat dependent on judgment but slight variations in effective length and average moment of inertia were found to have negligible effect. A sketch of these three representations of the haunch is given in Figure 22. In Model B the shaded area represents that portion of the haunch assumed rigid.

Influence lines for midspan moments, midspan deflections, and haunch connection moments were determined for all three of these haunch modeling assumptions. These are presented in Figures 23-26. In these figures the flexible model is labeled Model A. The rational model is identified as Model B and the extremely stiff haunch representation is labeled Model C. While these differences in assumptions of haunch stiffness do have an effect on moments and deflections, the effect is not as significant as might be expected from the extreme variations in the stiffness assumptions made. Thus, it may be concluded that any stiffness approximation of the haunch which is based on rational assumptions of the actual haunch configuration would yield results very close to those obtained using the particular model adopted in this study.

4. SUMMARY AND CONCLUSIONS

This relatively new slant leg, rigid frame, highway bridge design appears to be an entirely adequate type from both experimental and theoretical stress analysis considerations. Further, the test structure, completed in 1969 and in service approximately 6 years at the writing of this report, is in a good state of repair and appears to have at least a normal period of useful service in its future.

The particular conclusions drawn from this study may be summarized as follows:

1. The flexural stresses in the five frames were very sensitive to the transverse position of the test vehicle on the concrete deck. Further, the midspan deflections reflected the transverse position of the test vehicle. As has also been demonstrated in studies of simple beam composite deck and steel stringers, live loads on the decks are by no means carried equally by the several components of the superstructure. However, the AASHTO specifications for lateral distribution to stringers are highly conservative as design guides.

2. The live load stresses as experimentally determined were small compared to live load stresses calculated in the design.

3. An harmonic theory developed by A. W. Hendry and L. G. Jaeger and published in the ASCE, Proceedings, 82, No. ST4, pp. 1023-1 to 1023-48 (1956) provided a theoretical means of predicting relatively accurately the distribution of live loads to the longitudinal stringers in this test structure.

4. The estimated values of "n", the ratio of moduli of elasticity of steel to concrete, and the effective width of the composite concrete slab have only a small effect on the section modulus of the bottom fibers. Any reasonable estimates for these design parameters are very satisfactory for bridges of this type.

5. Influence diagrams for moments and deflections were not appreciably affected by various modelings of the haunch in the finite element analysis.

6. Influence diagrams for midspan moments and deflections were not appreciably affected by various support condition assumptions at the abutments and slant legs; however, the influence diagrams for moments at either face of the haunch were greatly affected by the above mentioned support conditions.

ACKNOWLEDGMENTS

The experimental phase of this study required the cooperation of many persons with both the Virginia Department of Highways and Transportation and the Federal Highway Administration. In particular, the authors express their appreciation to J. N. Clary, F. H. Stairs, Jr., and Robert G. Warner of the Virginia Department of Highways & Transportation, and C. F. Galambos, W. L. Armstrong, Jerry Nashanian, and Harry Laatz of the Federal Highway Administration. C. U. Moore of Hayes, Seay, Mattern and Mattern developed the original design of the test structure and cooperated with the authors throughout the study.

The research project was conducted under the general supervision of Jack H. Dillard, Head, Virginia Highway & Transportation Research Council. W. T. McKeel, Jr., Head, Structures Research Section of the Council, not only actively participated in the experimental phase of the project but offered valuable suggestions both during the theoretical study and the preparation of the report. In addition, R. K. Shearin and Victor Perry, both undergraduate civil engineering students at the University of Virginia, contributed significantly to the study in the theoretical analysis, the development of computer programs, and the preparation of influence diagrams and graphical depictions of the results.

REFERENCES

1. Standard Specifications for Highway Bridges, AASHTO, 1965.

2. Hendry, A. W., and L. G. Jaeger, "Load Distribution in Highway Bridge Decks", Proceedings, ASCE, 82, No. ST4, pp. 1023-1-1023-48 (1956).

3. Sanders and Ellerby, "Distribution of Wheel Loads on Highway Bridges", National Cooperative Highway Research Program, Report No. 83, 1970.

TABLE 1

TABULATIONS OF RUNS

Lane	Nominal Speed - mph (1 mph = 0.447 m/s)					
	Crawl	15	30	40	50	60
1	2	1	1	1	1	1
2	2	1	1	1	1	1
3	2	1	1	1	1	1
4	2	1	1	1	1	1
5	2	1	1	1	1	1

TOTAL 35 runs

TABLE 2

COORDINATES OF HAUNCH GAGES - inches (1 in. = 0.0254 m)
ORIGIN AT WORKING POINT - See Figure 6

GAGE	X	Y	GAGE	X	Y
S1	-48.4	-29.7	U4	29.8	21.0
S2	-28.0	-18.0	U5	54.4	21.0
S3	-7.3	-39.7	U6	78.9	21.0
S4	-23.9	-22.2	L1	-100.8	-16.7
S5	11.0	-26.3	L2	-76.4	-19.8
R1	-53.3	6.0	L3	-57.8	-31.2
R2	-53.3	6.0	L4	-52.2	-53.1
R3	-54.3	-7.0	L5	-60.3	-70.9
R4	-29.7	-33.4	L6	-31.5	-87.9
R5	-31.4	-50.1	L7	-14.9	-61.5
R6	-12.7	-10.0	L8	-1.8	-45.5
R7	29.3	6.0	L9	14.9	-33.3
R8	28.8	-6.0	L10	34.1	-25.6
U1	-100.8	21.0	L11	58.1	-23.0
U2	-73.2	21.0	L12	79.1	-23.0
U3	-33.8	21.0			

TABLE 3

DISTRIBUTION OF LIVE LOAD STRESSES - BOTTOM FLANGE - MIDSPAN

Test Vehicle in Lane (1)	Frame (2)	Composite Mom. of Inertia Inches[4] (3)	N.A. From Bottom Fiber Inches (4)	Exper. Stress psi (5)	Exper. Resist. Mom. Ft. Kips (6)	Exper. Mom. Distribution % (7)	Theor. Mom. Distribution % Harmonic Analysis (8)	Theor. Applied Mom. Ft. Kips (9)	Exper. Mom. Theor. Mom. % (10)
1	1	64,700	39.7	1555	211.2	24.53	24.24	227.3	
	2	"	"	2465	334.7	38.87	39.92	359.6	
	3	"	"	1570	213.2	24.76	21.48	193.5	
	4	"	"	620	84.2	9.78	10.55	95.1	
	5	"	"	130	17.7	2.06	2.81	25.3	
					861.0	100.00	100.00	900.8	95.6
2	1	64,700	39.7	1195	162.3	19.14	17.50	157.6	
	2	"	"	2150	292.0	34.43	34.58	311.5	
	3	"	"	1855	251.9	29.70	30.47	274.5	
	4	"	"	845	114.8	13.53	13.37	120.4	
	5	"	"	200	27.2	3.20	4.08	36.8	
					848.2	100.00	100.00	900.8	94.2
3	1	64,700	39.7	905	122.9	13.65	12.64	113.8	
	2	"	"	1990	270.2	30.01	30.68	276.4	
	3	"	"	2225	302.2	33.56	34.10	307.2	
	4	"	"	1115	151.4	16.82	16.65	150.0	
	5	"	"	395	53.6	5.96	5.93	53.4	
					900.3	100.00	100.00	900.8	99.9
4	1	64,700	39.7	400	54.3	6.12	8.77	79.0	
	2	"	"	1315	178.6	20.11	20.78	187.2	
	3	"	"	2225	302.2	34.02	40.94	368.8	
	4	"	"	1740	236.3	26.60	20.90	188.3	
	5	"	"	860	116.8	13.15	8.61	77.5	
					888.2	100.00	100.00	900.8	98.6
5	1	64,700	39.7	75	10.2	1.15	2.81	25.3	
	2	"	"	685	93.0	10.51	10.55	95.0	
	3	"	"	1500	203.7	23.03	21.48	193.5	
	4	"	"	2440	331.4	37.45	39.92	359.6	
	5	"	"	1815	246.5	27.86	25.24	227.4	
					884.8	100.00	100.00	900.8	98.2

Notes: 1 in.^{4} = 416.3 x 10^{-9} m^4
1 in. = 0.0254 m
1 psi = 6895 Pa
1 Ft.-kip = 9.417 N·m

Column No.

1. Location of test vehicle on structure by lane.
2. Frame number for data on that line.
3. Composite moment of inertia. n = 6; b = 12t + w_{fl} = 96 + 14 = 110". See Table 15.
4. c = distance from neutral axis to extreme fiber for same data as in (3).
5. Experimental stress from strain gages. Average for two runs.
6. Experimental resisting moment in ft. kips from $M = \frac{fI}{c}$ using data from columns 3, 4, and 5.
7. Percentages of moments in column 6.
8. Percentage of moments in column 8. 900.82 ft.-kips (1.2215 x 10^6 N·m) is the maximum live load moment at the midspan using the influence diagram in Figure 14 for moment at that position.
9. Theoretical moment in each beam from harmonic analysis theory.
10. Ratio of Experimental Moment (column 6) to Theoretical Moment (column 9).

TABLE 4

UPPER FLANGE MIDSPAN STRESSES
EXPERIMENTALLY MEASURED PEAK
COMPRESSIVE STRESSES - psi (1 psi = 6895 Pascals)

	Lane of Test Vehicle				
	1	2	3	4	5
Frame 2	235	265	235	150	95

NOTES: Upper flange gages placed on Frame 2 only
See Figure 7 for gage locations.

TABLE 5

HAUNCH GAGES

Gages on Stiffeners
Peak Tensile Stresses - psi (1 psi = 6895 Pascals)

Gage	Lane of Test Vehicle				
	1	2	3	4	5
S1*	765	690	580	310	140
S2*	610	570	460	230	130
S3*	470	500	430	310	170
S4*	270	290	300	190	120
S5*	500	510	470	350	170

Note: See Figure 6 for gage locations.

TABLE 6

HAUNCH GAGES

Gages on Lower Flanges
Peak Compressive Stresses - psi (1 psi = 6895 Pascals)

Gage	Lane of Test Vehicle				
	1	2	3	4	5
L1	1280	1260	1120	770	380
L2	860	790	730	530	270
L3	1900	1800	1550	960	270
L4	2280	2290	1870	1210	400
L5	1470	1390	1110	700	200
L6	1740	1660	1590	1120	530
L7	1680	1610	1510	1040	520
L8	1220	1170	1040	720	320
L9	1290	1210	1140	760	340
L10	1580	1500	1390	960	430
L11	1580	1520	1340	1800	410
L12*	1360	1310	1160	740	400

Note: See Figure 6 for gage locations.

TABLE 7

HAUNCH GAGES

Gages on Upper Flange
Peak Tensile Stresses - psi (1 psi = 6895 Pascals)

Gage	Lane of Test Vehicle				
	1	2	3	4	5
U1	270	360	130	40	50
U2	200	150	120	50	40
U3	170	190	150	60	40
U4	200	280	100	40	10
U5*	170	260	80	80	30
U6*	160	240	90	40	20

Note: See Figure 6 for gage locations.

TABLE 8

PEAK MIDSPAN DEFLECTIONS - inches (1 inch = 0.0254 m)
and
LOAD DISTRIBUTION TO FRAMES BASED ON PEAK DEFLECTIONS

Lane of Test Vehicle	Frame Number										Sum of Deflections of Five Frames
	1		2		3		4		5		
	Def.	Load Dist.	Def.	Load Dist.	Def.	Load Dist.	Def.	Load Dist.	Def.	Load Dist.	
1	0.23	29.5	0.23	29.5	0.21	26.9	0.10	12.8	0.01	1.3	0.78
2	0.17	21.5	0.23	29.1	0.24	30.4	0.12	15.2	0.03	3.8	0.79
3	0.14	16.9	0.21	25.3	0.26	31.3	0.16	19.3	0.06	7.2	0.83
4	0.08	9.5	0.15	17.9	0.26	30.9	0.22	26.2	0.13	15.5	0.84
5	0.01	1.2	0.07	8.3	0.21	24.7	0.28	32.9	0.28	32.9	0.85

NOTES: See Figure 5 for frame identification and lane locations.

Load distribution is percentage of sum of deflections.

TABLE 9

PRINCIPAL STRESSES - psi (1 psi = 6895 Pascals) FROM ROSETTE GAGES ON HAUNCH WEB OF FRAME 2.

Gage	Maximum Value and Test Vehicle Location			Minimum Value and Test Vehicle Location		
Rosette 1	+849	Lane 1	48%	-415	Lane 1	34%
Rosette 2	+799	Lane 1	47%	-442	Lane 1	34%
Rosette 3	+1318	Lane 1	34%	-269	Lane 1	48%
Rosette 4	+1608	Lane 1	33%	-968	Lane 1	48%
Rosette 5	+1666	Lane 1	32%	-130	Lane 4	29%
Rosette 6	+959	Lane 1	32%	-630	Lane 2	30%
Rosette 7	+1369	Lane 1	42%	-143	Lane 2	47%
Rosette 8	+1808	Lane 1	42%	-111	Lane 5	27%

Notes: See Figure 6 for rosette gage locations.
See Figure 5 and 9 for vehicle position location.

TABLE 10

PRINCIPAL STRESSES (psi) FROM ROSETTE GAGES
ON HAUNCH TEST VEHICLE IN LANE 1
(1 psi = 6895 Pascals)

Rosette	Principal Stress and Direction	Test Vehicle Location						
		32%	33%	34%	35%	42%	47%	48%
1	σ_1	313	173	524	605	480	824	849
	σ_2	10	-140	-415	-218	124	22	- 10
	θ degrees	50.6 ccw	80.9 ccw	55.6 ccw	47.8 ccw	1.2 ccw	22.4 cw	24.1 cw
2	σ_1	232	288	273	260	440	799	767
	σ_2	-173	-365	-442	-299	48	0	7
	θ degrees	67.1 cw	70.8 cw	75.0 cw	60.2 ccw	2.1 cw	18.2 cw	15.2 cw
3	σ_1	1207		1318	1095	868	1229	1218
	σ_2	465		100	457	- 4	-280	-269
	θ degrees	67.1 cw	45.3 cw	56.4 cw	74.1 cw	37.4 ccw	31.4 ccw	31.2 ccw
4	σ_1	1598	1608	1521	1454	926	1244	1241
	σ_2	-382	-285	-257	-166	-278	-887	-968
	θ degrees	56.4 ccw	58.4 ccw	62.4 ccw	67.5 ccw	30.9 ccw	19.0 ccw	18.5 ccw
5	σ_1	1663	1666	1621	1418	828	811	821
	σ_2	- 71	- 25	18	123	534	204	182
	θ degrees	46.9 cw	45.8 cw	42.6 cw	38.0 cw	37.6 cw	89 ccw	88.8 ccw
6	σ_1	959	908	898	1141	817	668	672
	σ_2	-259	-248	132	-141	401	83	62
	θ degrees	31.1 ccw	31.0 ccw	37.7 ccw	43.8 ccw	57.3 ccw	20.9 cw	19.4 cw
7	σ_1	401	418	418	699	1369	750	687
	σ_2	88	12	12	238	445	80	132
	θ degrees	30.4 ccw	35.4 ccw	35.4 ccw	55.5 ccw	56 ccw	50.2 ccw	50.2 ccw
8	σ_1	660	667	642	893	1808	1383	1311
	σ_2	429	409	361	440	388	984	1080
	θ degrees	19.2 cw	11.0 cw	4.5 cw	43.5 ccw	42.8 ccw	44.7 ccw	50.9 ccw

Notes: See Figure 6 for rosette gage locations.
See Figure 9 for test vehicle location.

TABLE 11

PRINCIPAL STRESSES (psi) FROM ROSETTE GAGES
ON HAUNCH TEST VEHICLE IN LANE 2
(psi = 6895 Pascals)

Rosette	Principal Stress and Direction	Test Vehicle Location				
		30%	31%	34%	47%	48%
1	σ_1	421	513	169	738	791
	σ_2	- 8 cw	- 46	- 45	17	23
	θ degrees	44.2 ccw	45.9 ccw	72.6 ccw	23.1 cw	23.0 cw
2	σ_1	222	228	397	667	712
	σ_2	- 22	-127	-162	41	15
	θ degrees	66.2 ccw	66.7 ccw	61.4 cw	14.8 cw	14.2 cw
3	σ_1	1031	1086	1176	1081	1156
	σ_2	388	381	170	-228	-242
	θ degrees	85.1 cw	79.5 cw	56.3 cw	31.8 ccw	31.4 ccw
4	σ_1	1487	1549	1564	998	1048
	σ_2	-378	-271	-285	-444	-507
	θ degrees	51.7 ccw	53.8 ccw	58.2 cw	7.9 ccw	6.9 ccw
5	σ_1	1496	1582	1609	783	817
	σ_2	- 90	- 55	26	323	289
	θ degrees	51.4 cw	50.0 cw	47.2 cw	89.0 ccw	87.o ccw
6	σ_1	848	858	914	580	602
	σ_2	-630	-629	-503	225	163
	θ degrees	27.2 ccw	27.2 ccw	31.2 ccw	2.6 cw	13.1 cw
7	σ_1	306	300	402	896	796
	σ_2	- 36	- 31	- 3	-143	- 43
	θ degrees	7.6 ccw	7.9 ccw	34.4 ccw	46.9 ccw	46.5 ccw
8	σ_1	662	674	572	1320	1284
	σ_2	75	100	298	729	899
	θ degrees	35.5 cw	36.3 cw	24 cw	42.8 ccw	45.9 ccw

Notes: See Figure 6 for rosette gage locations.
See Figure 9 for test vehicle location.

TABLE 12

PRINCIPAL STRESSES (psi) FROM ROSETTE GAGES
ON HAUNCH TEST VEHICLE IN LANE 3
(1 psi = 6895 Pascals)

Rosette	Principal Stress and Direction	Test Vehicle Location				
		30%	34%	48%	49%	50%
1	σ_1	316	327	736	809	777
	σ_2	- 91	-309	- 27	- 43	- 55
	θ degrees	49.7 ccw	55.7 ccw	25.0 cw	26.6 cw	26.1 cw
2	σ_1	161	283	677	697	660
	σ_2	- 63	- 33	- 3	- 41	- 47
	θ degrees	70.2 ccw	71.8 ccw	17.8 cw	19.3 cw	20.5 cw
3	σ_1	807	801	1118	1085	1038
	σ_2	163	1	-207	-186	-224
	θ degrees	81.8 cw	65.0 cw	32.0 ccw	31.5 ccw	32.2 ccw
4	σ_1	1158	1067	964	927	924
	σ_2	-419	-123	-661	-720	-730
	θ degrees	53.6 ccw	60.6 ccw	7.1 ccw	6.8 ccw	6.8 ccw
5	σ_1	1132	1054	642	602	604
	σ_2	-100	26	126	69	68
	θ degrees	49.0 cw	41.8 cw	82.1 ccw	79.4 ccw	80.9 ccw
6	σ_1	706	633	541	567	590
	σ_2	-436	-272	64	21	- 12
	θ degrees	28.2 ccw	32.8 ccw	16.8 cw	22.4 cw	23.8 cw
7	σ_1	300	267	620	580	529
	σ_2	87	2	156	232	294
	θ degrees	2.8 cw	29.8 ccw	48.9 ccw	46.5 ccw	46.4 ccw
8	σ_1	447	392	1140	1090	1157
	σ_2	97	189	996	1010	1029
	θ degrees	27.0 cw	15.6 cw	49.7 ccw	74.3 ccw	76.9 cw

Notes: See Figure 6 for rosette gage locations.
See Figure 9 for test vehicle location.

TABLE 13

PRINCIPAL STRESSES (psi) FROM ROSETTE GAGES
ON HAUNCH TEST VEHICLE IN LANE 4
(1 psi = 6895 Pascals)

Rosette	Principal Stress and Direction	Test Vehicle Location						
		28%	29%	31%	48%	49%	52%	53%
1	σ_1	309	311	295	548	568	575	546
	σ_2	- 69	- 62	-118	30	- 8	- 22	- 21
	θ degrees	43.8 ccw	44.2 ccw	48.0 ccw	22.0 cw	24.1 cw	25.6 cw	25.2 cw
2	σ_1	140	135	163	503	468	517	506
	σ_2	- 71	-102	- 69	19	6	- 7	- 8
	θ degrees	54.7 ccw	56.1 ccw	57.3 ccw	19.0 cw	19.9 cw	22.2 cw	22.2 cw
3	σ_1	522	548	547	790	780	789	789
	σ_2	107	117	107	-148	-163	-111	-111
	θ degrees	84.6 ccw	86.1 ccw	81.4 cw	31.8 ccw	32.3 ccw	31.0 ccw	31.0 ccw
4	σ_1	743	769	790	675	672	672	612
	σ_2	-461	-416	-364	-493	-502	-538	-573
	θ degrees	49.8 ccw	52.1 ccw	53.0 ccw	7.5 ccw	7.3 ccw	6.3 ccw	7.7 ccw
5	σ_1	540	618	570	448	444	435	426
	σ_2	-124	-130	-119	17	- .4	- 56	- 71
	θ degrees	56.4 cw	53.5 cw	51.7 cw	79.1 ccw	78.6 ccw	77.6 ccw	76.9 ccw
6	σ_1	398	414	413	437	417	433	403
	σ_2	-358	-345	-334	64	27	- 23	- 33
	θ degrees	26.4 ccw	27.0 ccw	28.1 ccw	25.1 cw	23.2 cw	24.4 cw	25.1 cw
7	σ_1	124	142	121	479	442	376	344
	σ_2	- 10	- 4	- 18	107	156	222	218
	θ degrees	1.9 ccw	1.9 ccw	11.7 ccw	50.5 ccw	51.4 ccw	54.6 ccw	46.4 ccw
8	σ_1	152	142	163	859	861	844	799
	σ_2	- 32	- 33	- 18	659	682	736	674
	θ degrees	15.8 cw	15.4 cw	18.7 cw	51.7 ccw	54.7 ccw	83.7 cw	76.2 cw

Notes: See Figure 6 for rosette gage locations.
See Figure 9 for test vehicle location.

TABLE 14

PRINCIPAL STRESSES (psi) FROM ROSETTE GAGES
ON HAUNCH TEST VEHICLE IN LANE 5
(1 psi = 6895 Pascals)

Rosette	Principal Stress and Direction	Test Vehicle Location					
		27%	30%	50%	51%	52%	55%
1	σ_1	146	153	247	247	243	269
	σ_2	-129	-104	1	1	- 3	4
	θ degrees	49.0 ccw	48.4 ccw	21.7 cw	21.7 cw	21.0 cw	21.8 cw
2	σ_1	92	70	180	237	223	185
	σ_2	- 68	- 95	- 34	12	- 4	- 28
	θ degrees	52.1 ccw	54.3 ccw	15.9 cw	12.1 cw	6.5 cw	17.1 cw
3	σ_1	160	148	392	402	393	337
	σ_2	- 28	- 40	- 79	- 65	- 80	-109
	θ degrees	89.7 cw	89.8 cw	30.1 ccw	29.0 ccw	28.4 ccw	28.7 ccw
4	σ_1	190	183	337	337	334	298
	σ_2	-102	-106	-203	-203	-212	-188
	θ degrees	60.3 ccw	61.2 ccw	3.1 ccw	3.1 ccw	3.4 ccw	1.8 ccw
5	σ_1	133	124	260	258	239	213
	σ_2	- 17	- 20	50	39	33	36
	θ degrees	48.7 cw	50.2 cw	81.5 ccw	80.9 ccw	80.3 ccw	80.9 ccw
6	σ_1	98	98	201	193	225	204
	σ_2	-154	-154	18	14	5	- 9
	θ degrees	30.0 ccw	30.0 ccw	28.1 cw	23.8 cw	28.4 cw	28.7 cw
7	σ_1	- 15	- 15	147	137	138	123
	σ_2	- 84	- 84	- 69	- 47	- 72	33
	θ degrees	13.9 ccw	13.9 ccw	47.7 ccw	47.2 ccw	48.7 ccw	45.3 ccw
8	σ_1	24	7	362	371	392	352
	σ_2	-111	-106	298	301	304	272
	θ degrees	32.1 cw	31.4 cw	87.5 ccw	72.3 cw	71.3 cw	74.8 cw

Notes: See Figure 6 for rosette gage locations.
See Figure 9 for test vehicle location.

TABLE 15

NEUTRAL AXIS LOCATIONS AND MOMENTS OF INERTIA FROM ELASTIC THEORY CALCULATIONS

(1 inch - 0.0254 m)
(1 $in.^4$ - 4.16 x 10^{-7} m^4)
(1 in.-kip - 113 newton-metre)

	b = 12t + Flange Width	b = 12t	b = 12t + Flange Width	b = 12t
Theoretical C	39.7 in.	38.8 in.	37.7 in.	36.7 in.
Experimental C	39.3 in.	39.3 in.	39.3 in.	39.3 in.
Moment of Inertia	64,700 $in.^4$	62,800 $in.^4$	60,600 $in.^4$	58,600 $in.^4$
Resisting Moment	1630 in. kips	1620 in. kips	1610 in. kips	1600 in. kips

NOTES: "C" values locate neutral axis from bottom fiber. See Figure 13
Moments of Inertia are calculated from Theoretical "C" positions.

TABLE 16

MAXIMUM LOWER FLANGE MIDSPAN STRESSES - psi (1 psi = 6895 Pascal)
SIMULATED SIMULTANEOUS LOADING OF BOTH TRAFFIC LANES

	Frame Number				
Lane	1	2	3	4	5
Lane 3	905	1990	2225	1115	395
Lane 5	75	685	1500	2440	1815
TOTAL	980	2675	3725	3555	2210

NOTE: See Figure 7 for gage locations.

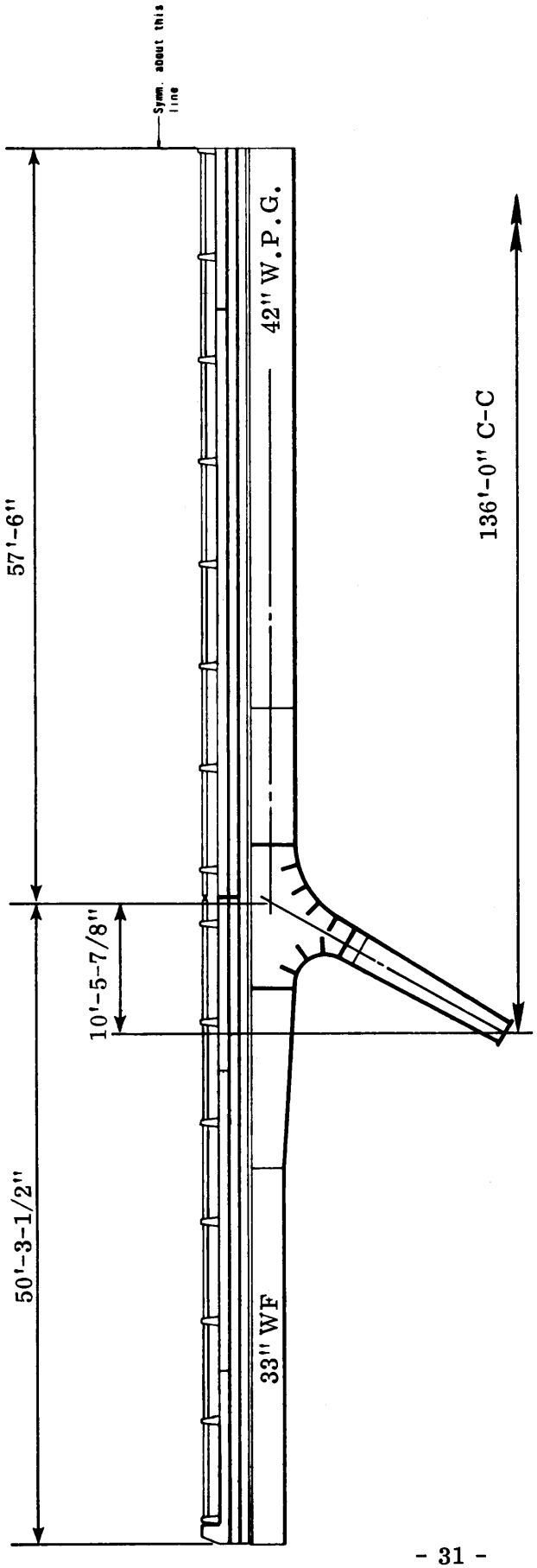

Figure 1. Partial elevation of test structure.

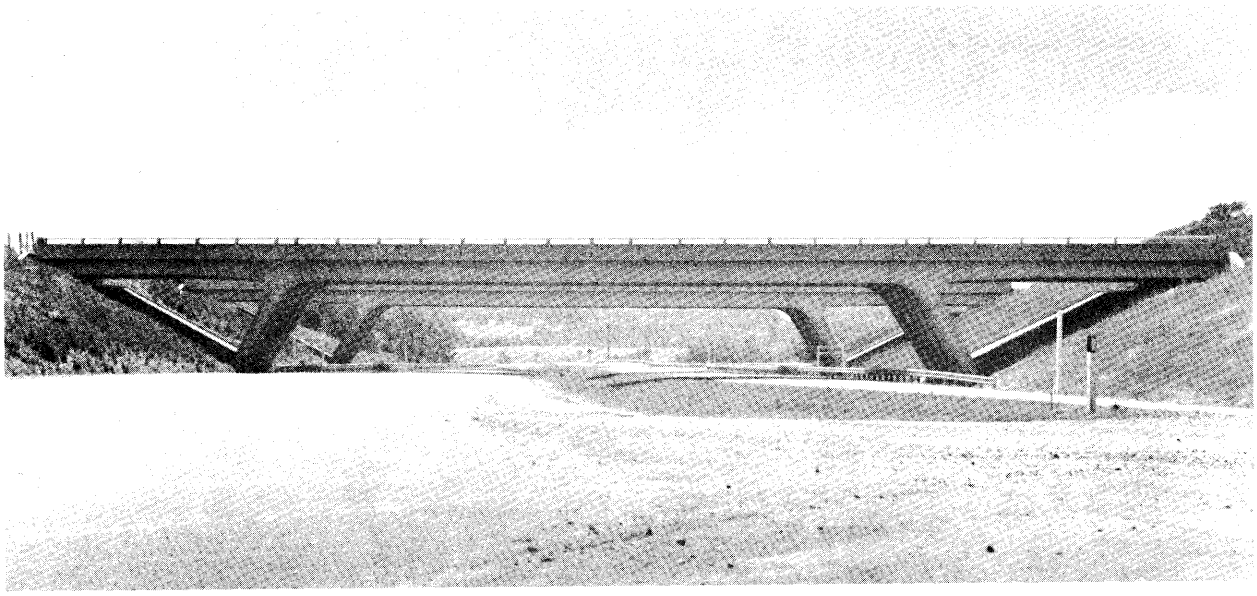

Figure 2. Test structure.

Figure 3. Test vehicle.

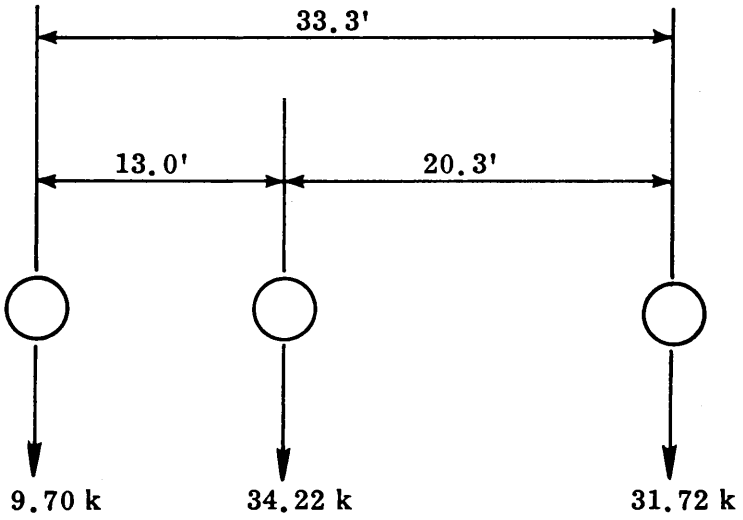

Axle Weights and Spacing

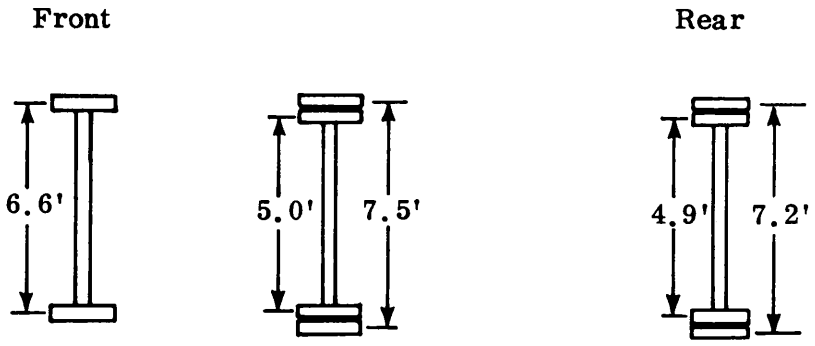

Wheel Spacing

Total Test Vehicle Weight = 75.64 k

Figure 4. Truck dimensions and axle weights.

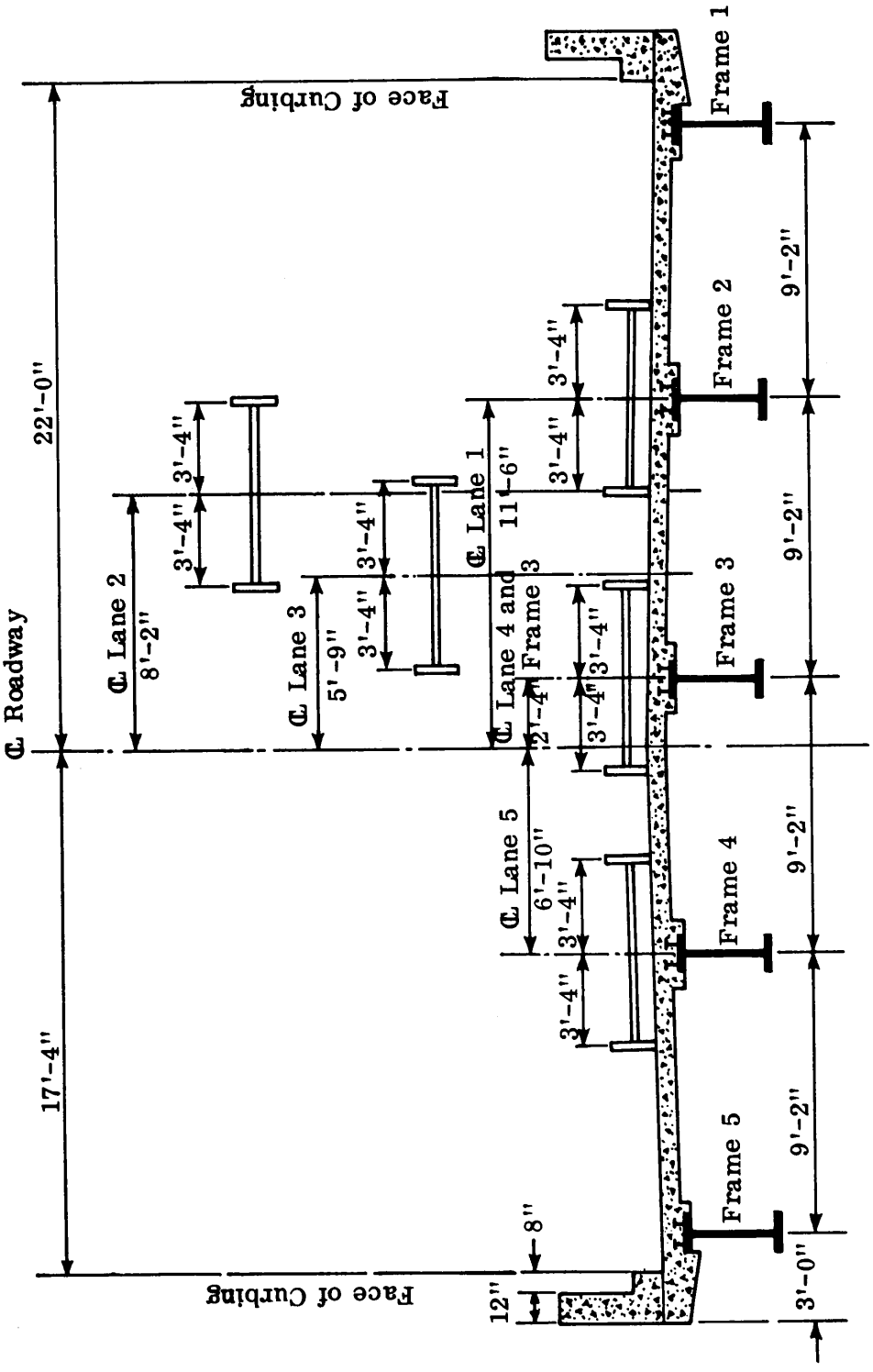

Looking West Toward Staunton

Figure 5. Transverse section and lane locations.

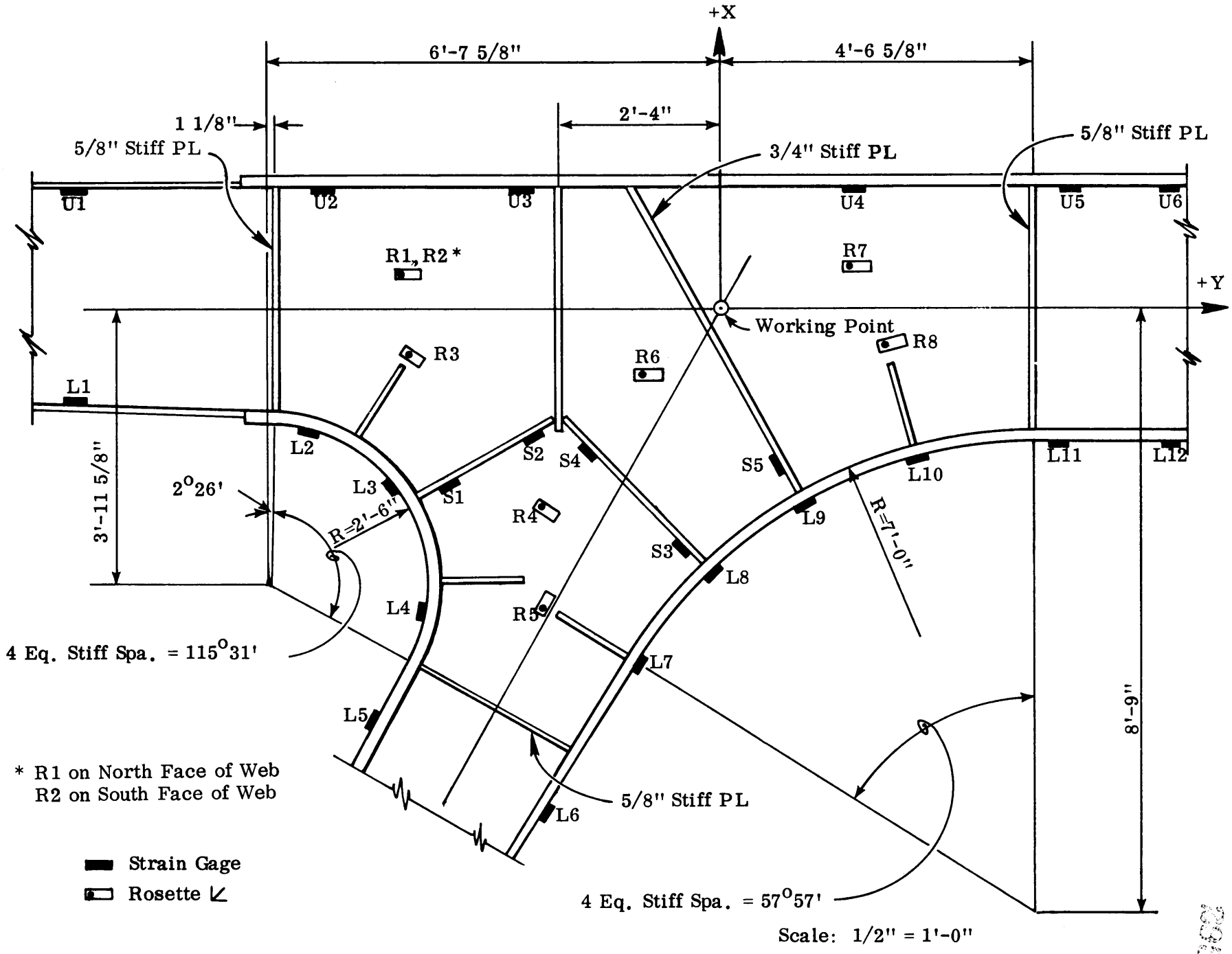

Figure 6. Haunch sketch showing gage locations.

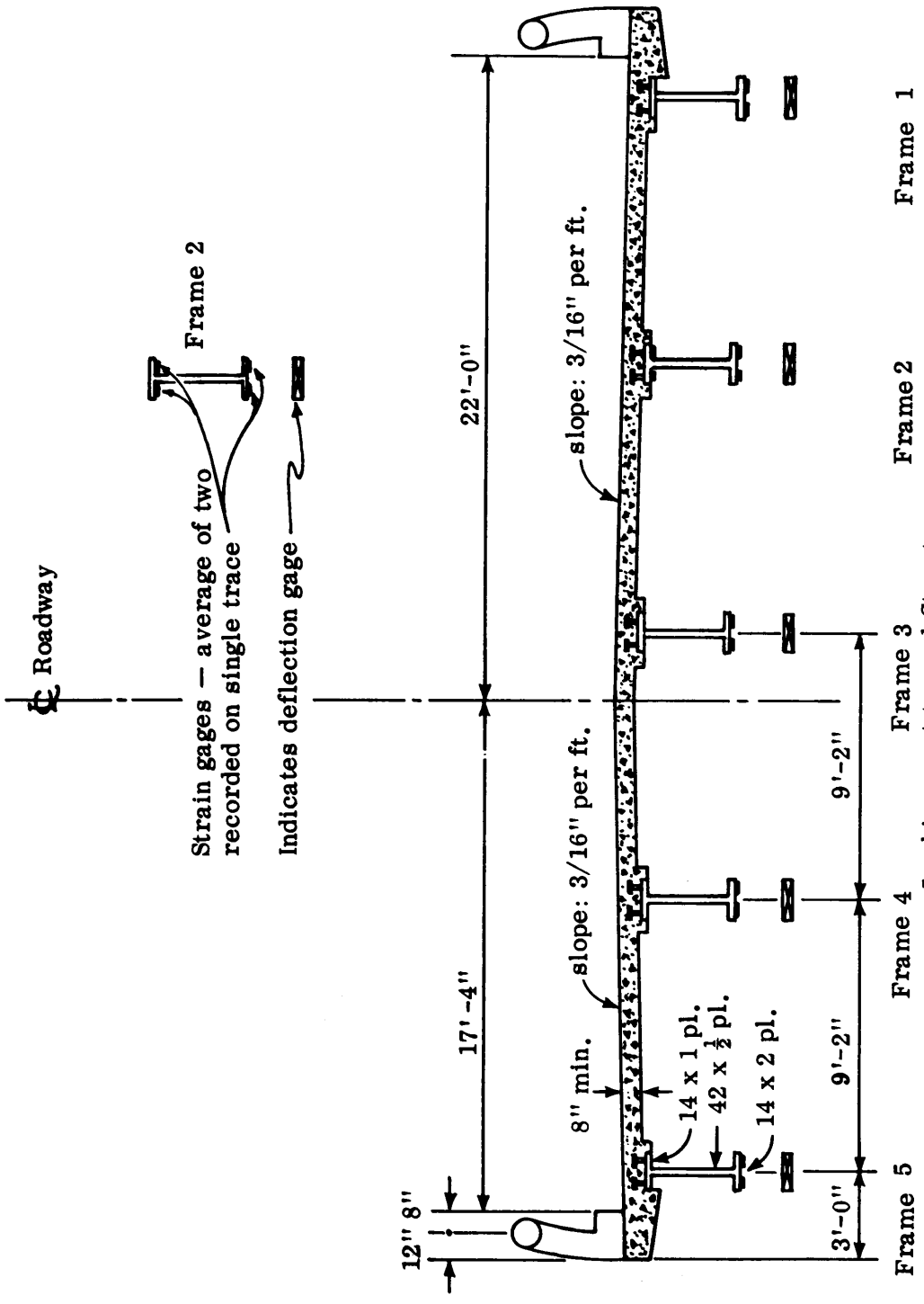

Figure 7. Section at midspan showing gage locations.

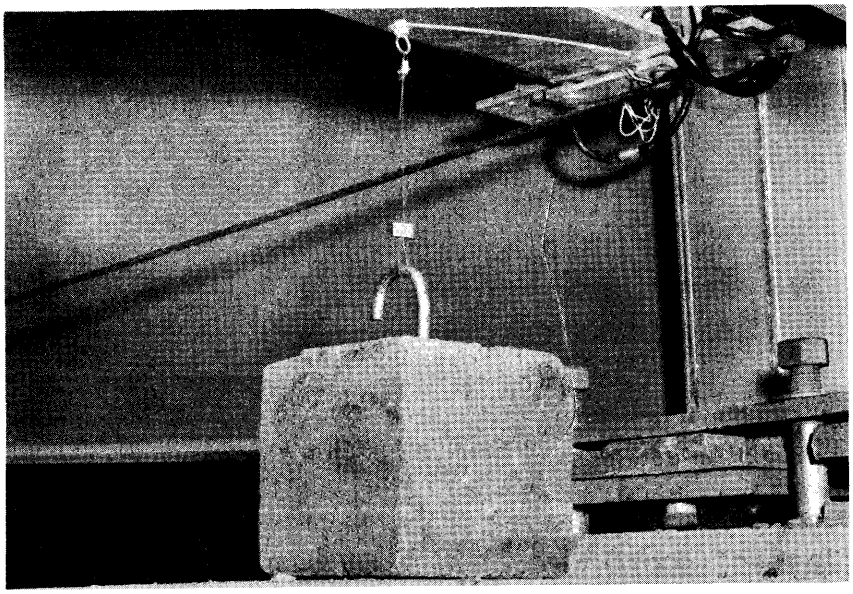

Figure 8. A typical deflection gage. (Gage is mounted on structure in earlier study.)

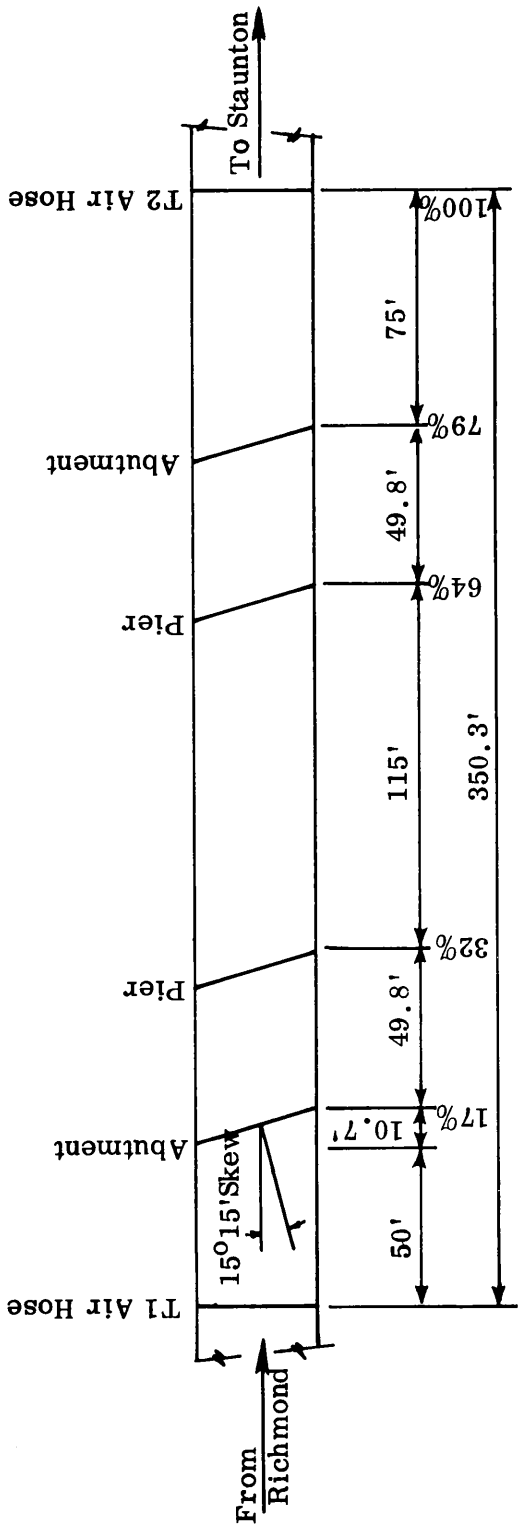

(Percentages indicate distances from T1 air hose to T2 air hose.)

Figure 9. Location of air hoses.

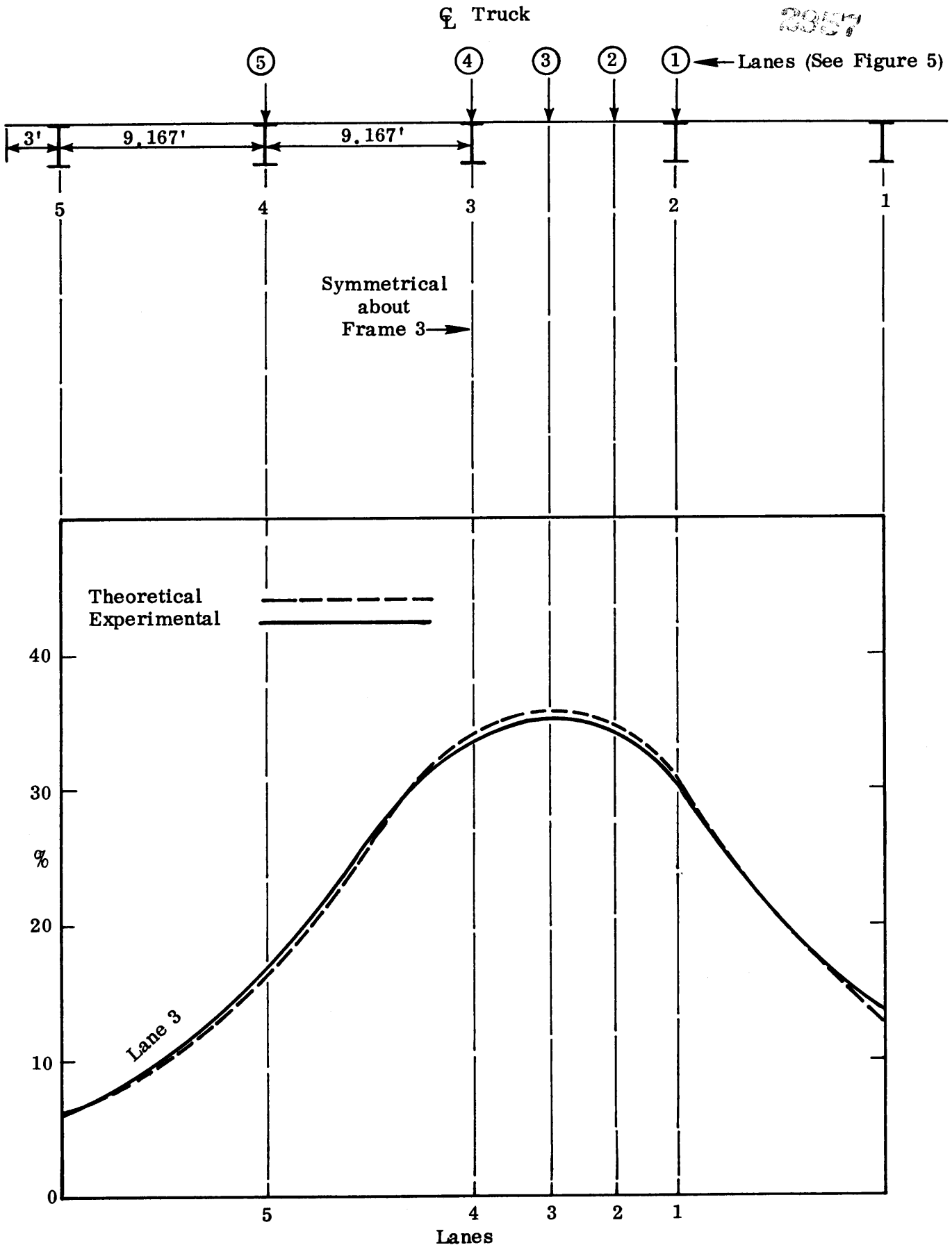

Figure 10. Distribution of loads for test vehicle in lane 3.

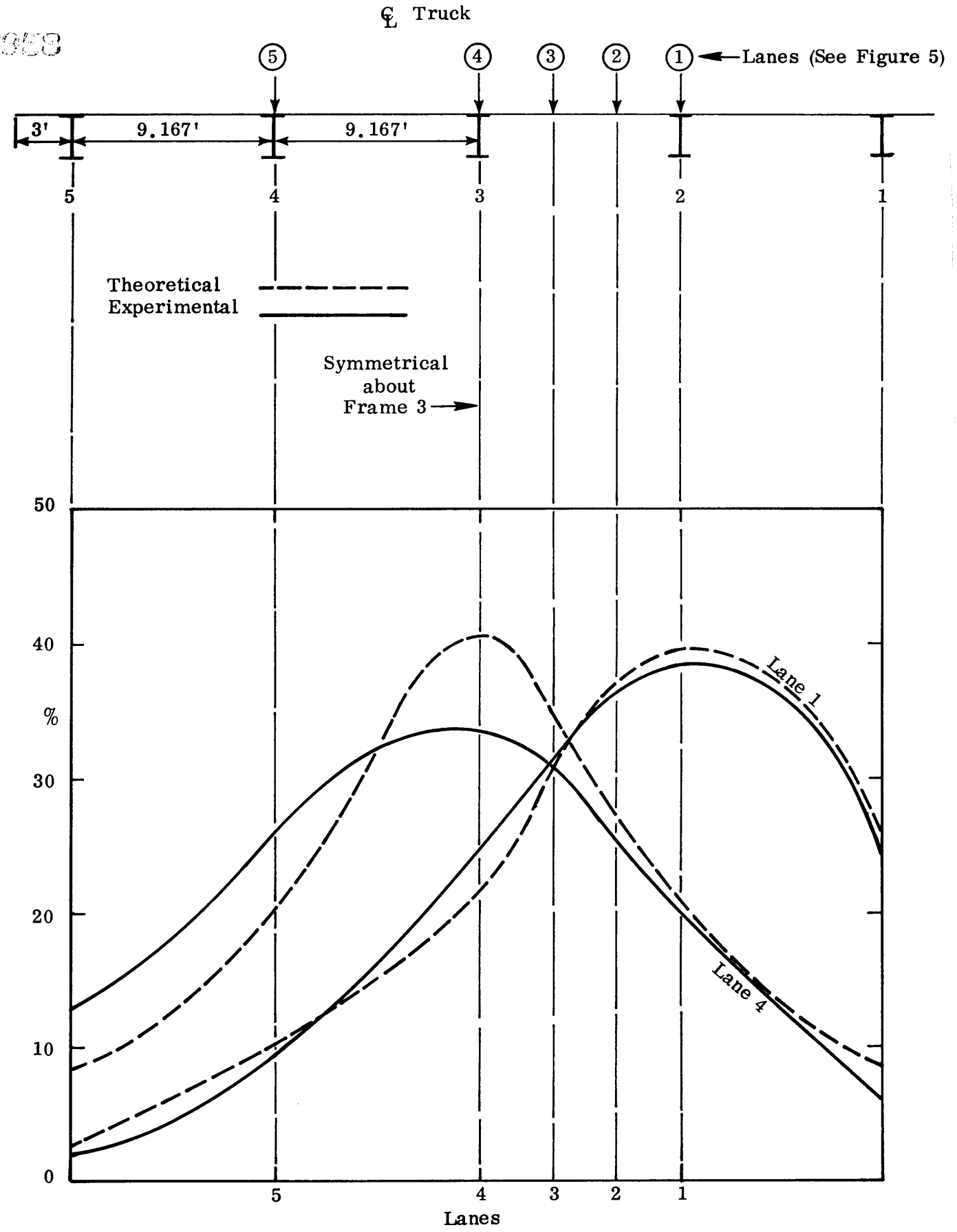

Figure 11. Distribution of loads for test vehicle in lanes 1 and 4.

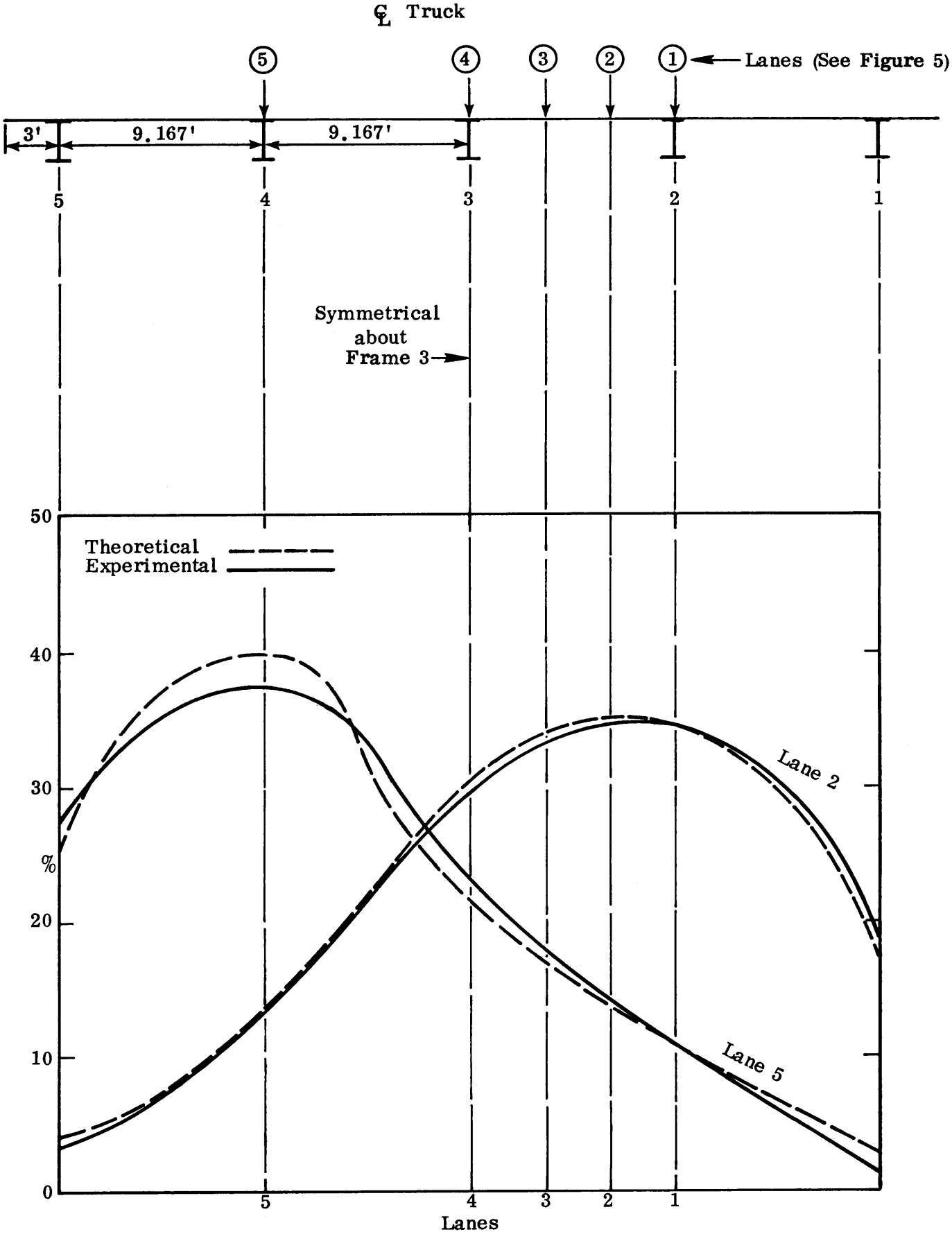

Figure 12. Distribution of loads for test vehicle in lanes 2 and 5.

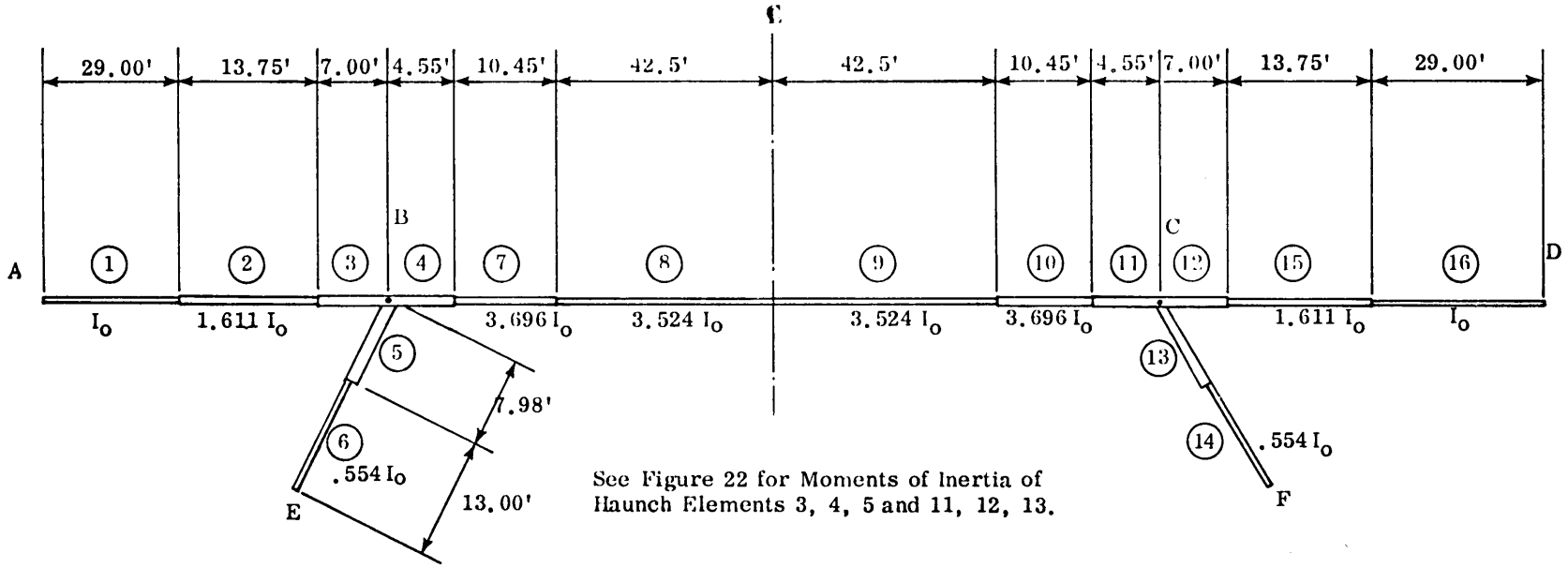

$I_o = 18,352$ in.^{4}

1 inch^4 = 416.3 x 10^{-9} m^4

Figure 13. Idealized model of rigid frame structure.

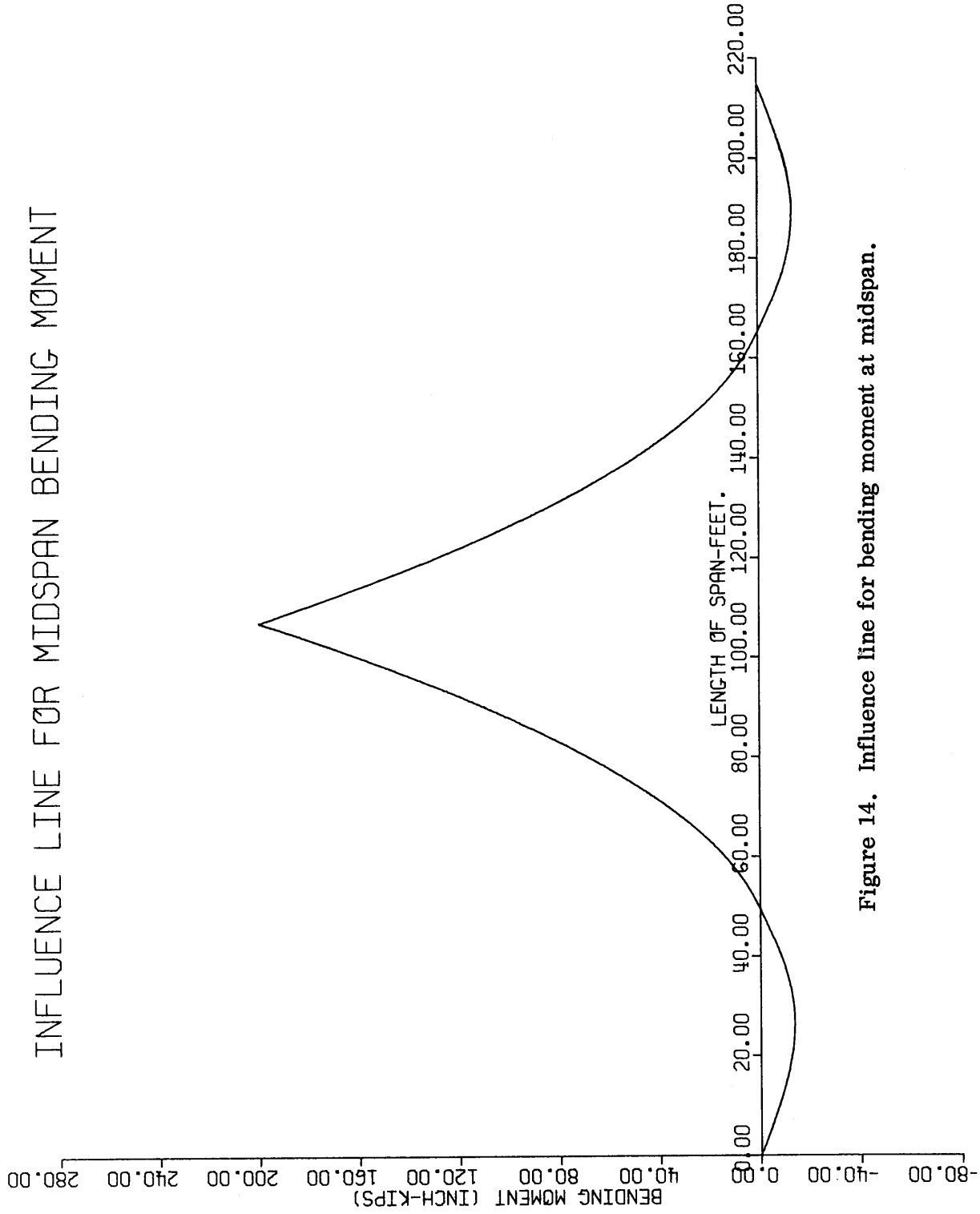

Figure 14. Influence line for bending moment at midspan.

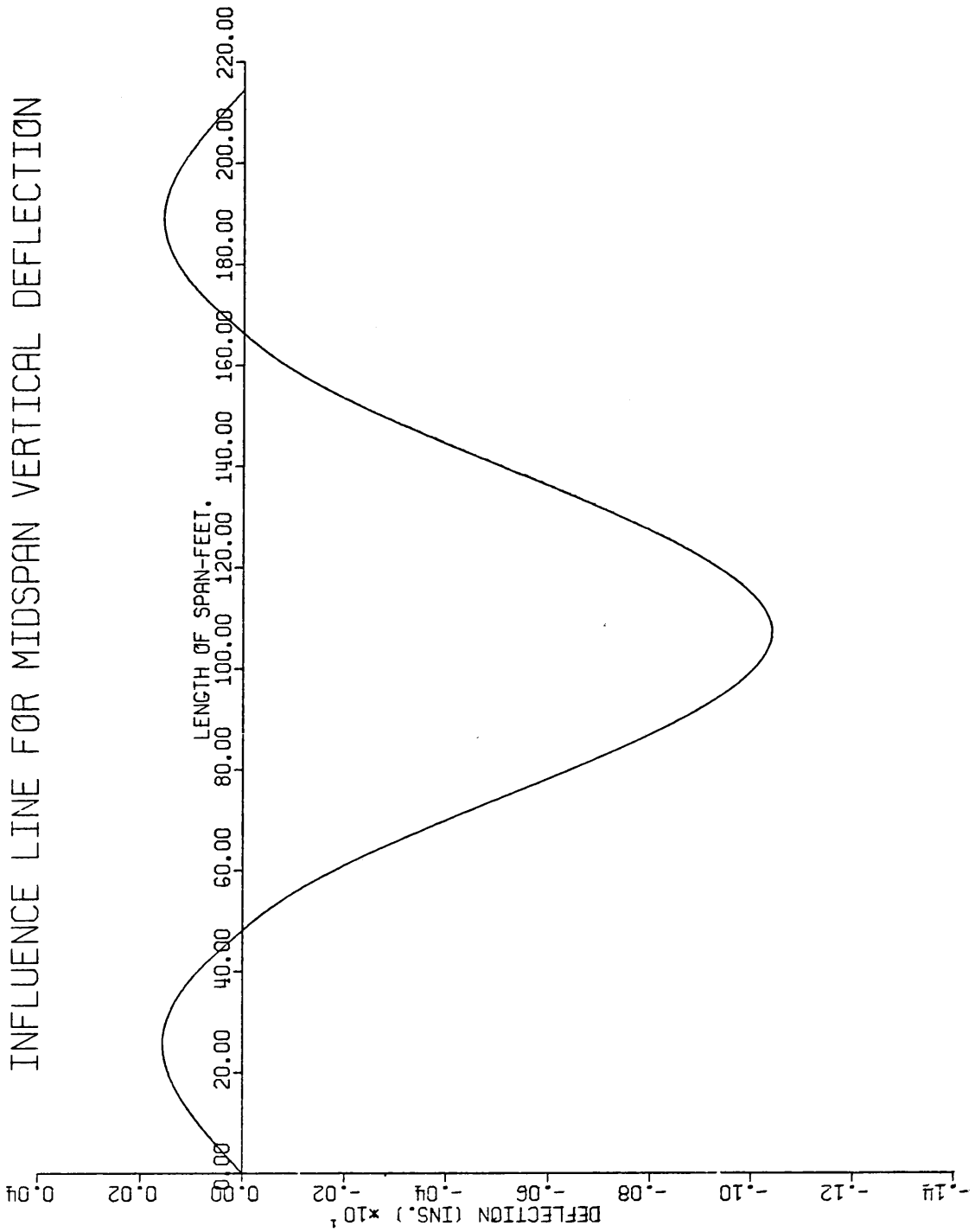

Figure 15. Influence line for deflection at midspan.

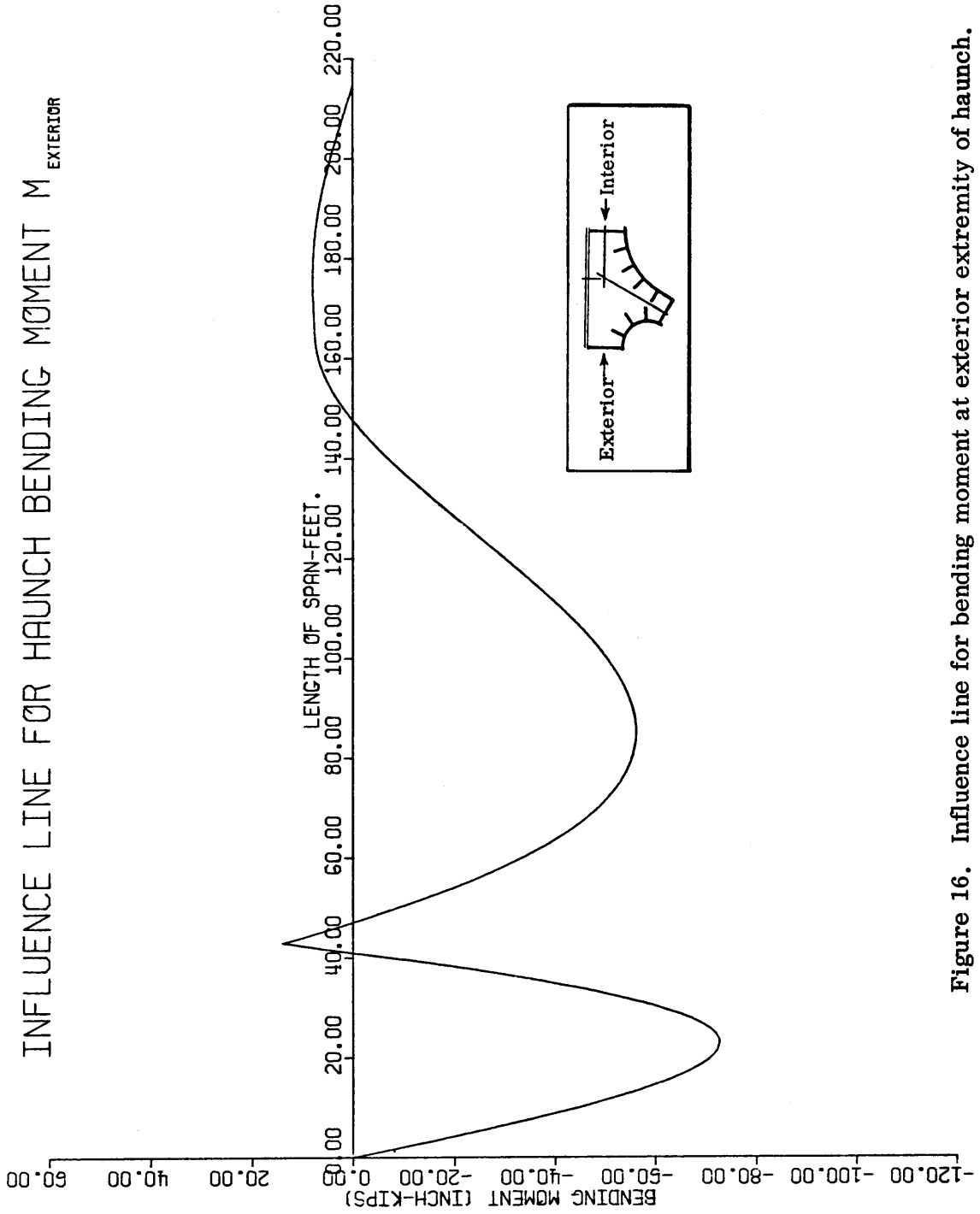

Figure 16. Influence line for bending moment at exterior extremity of haunch.

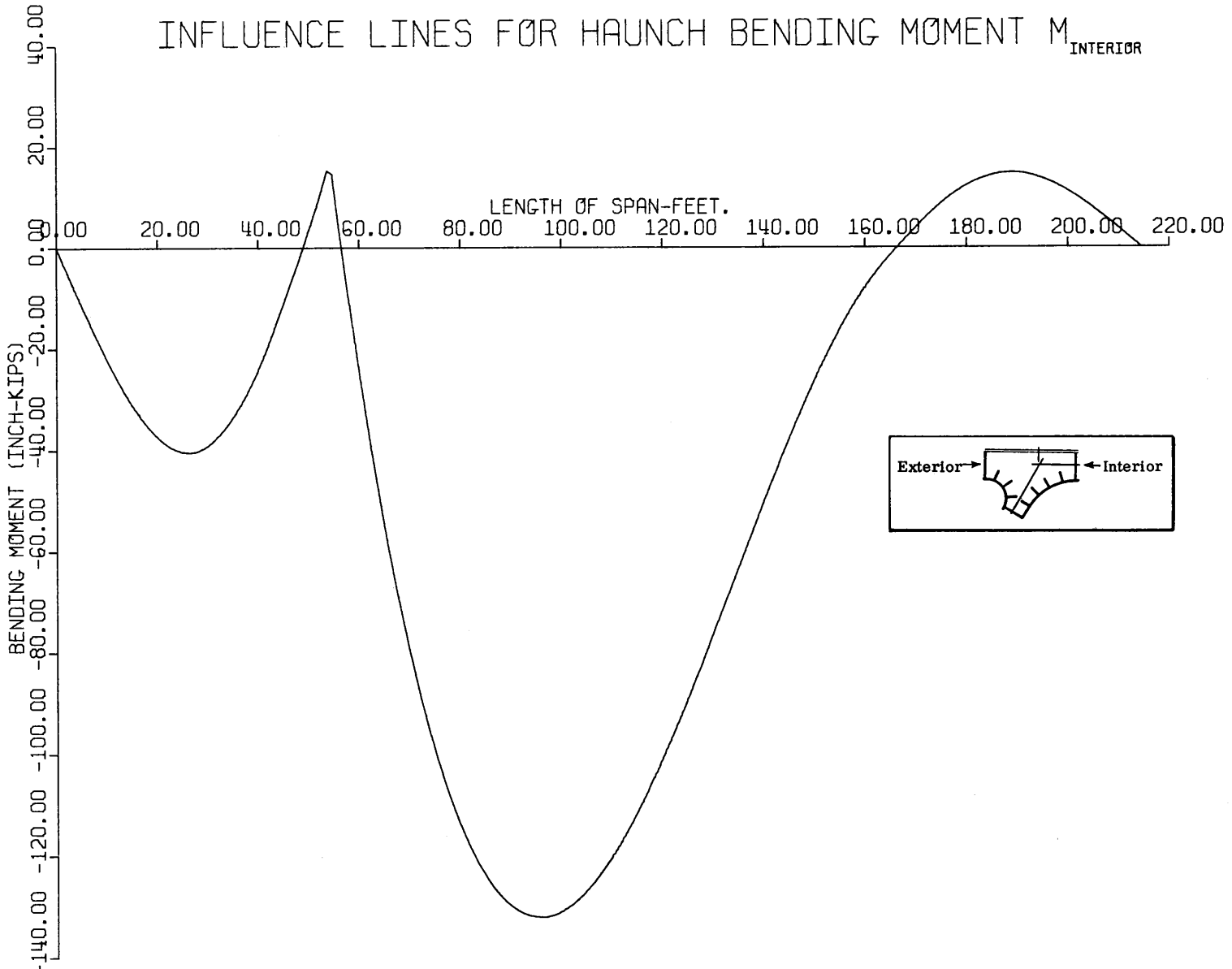

Figure 17. Influence line for bending moment at interior extremity of haunch.

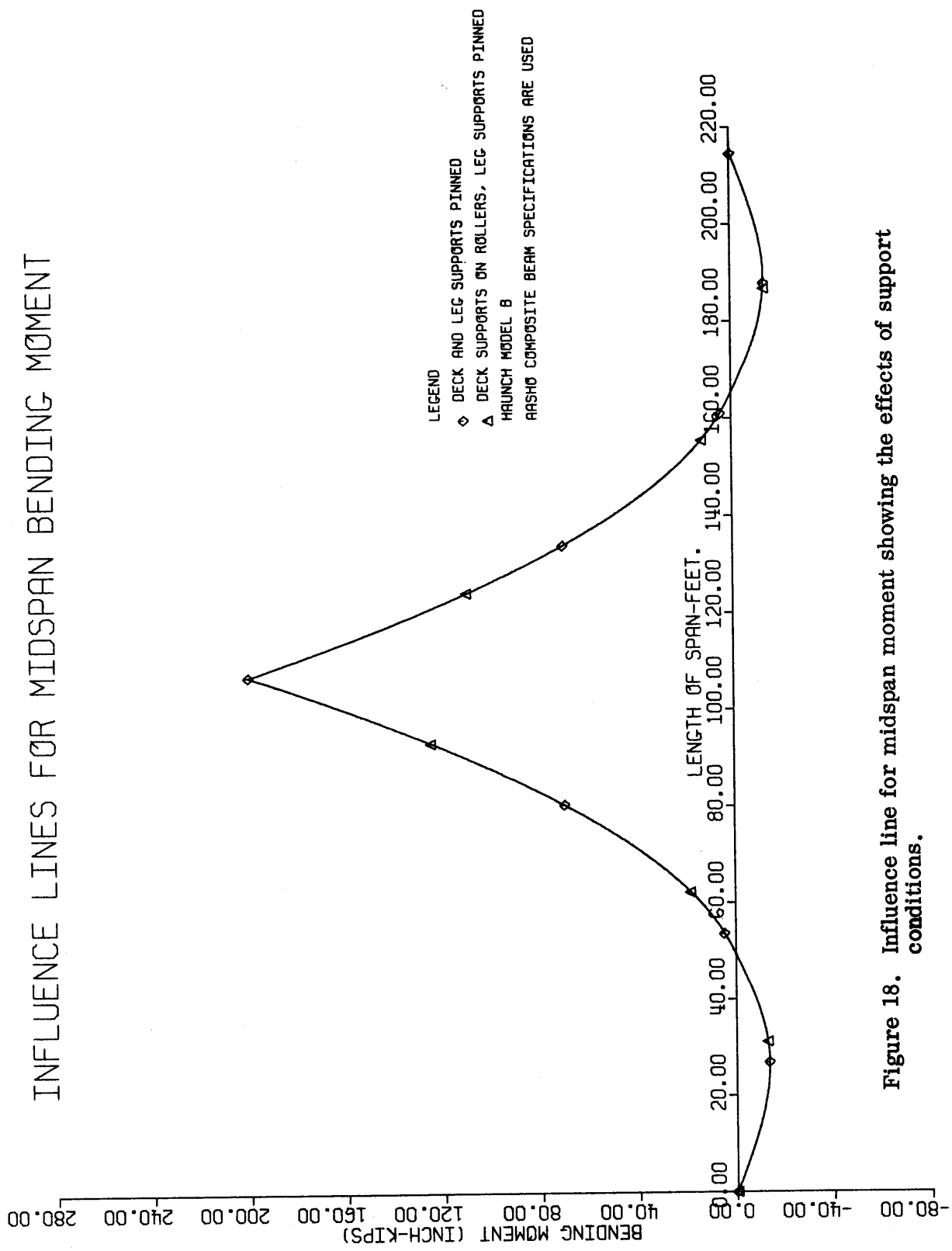

Figure 18. Influence line for midspan moment showing the effects of support conditions.

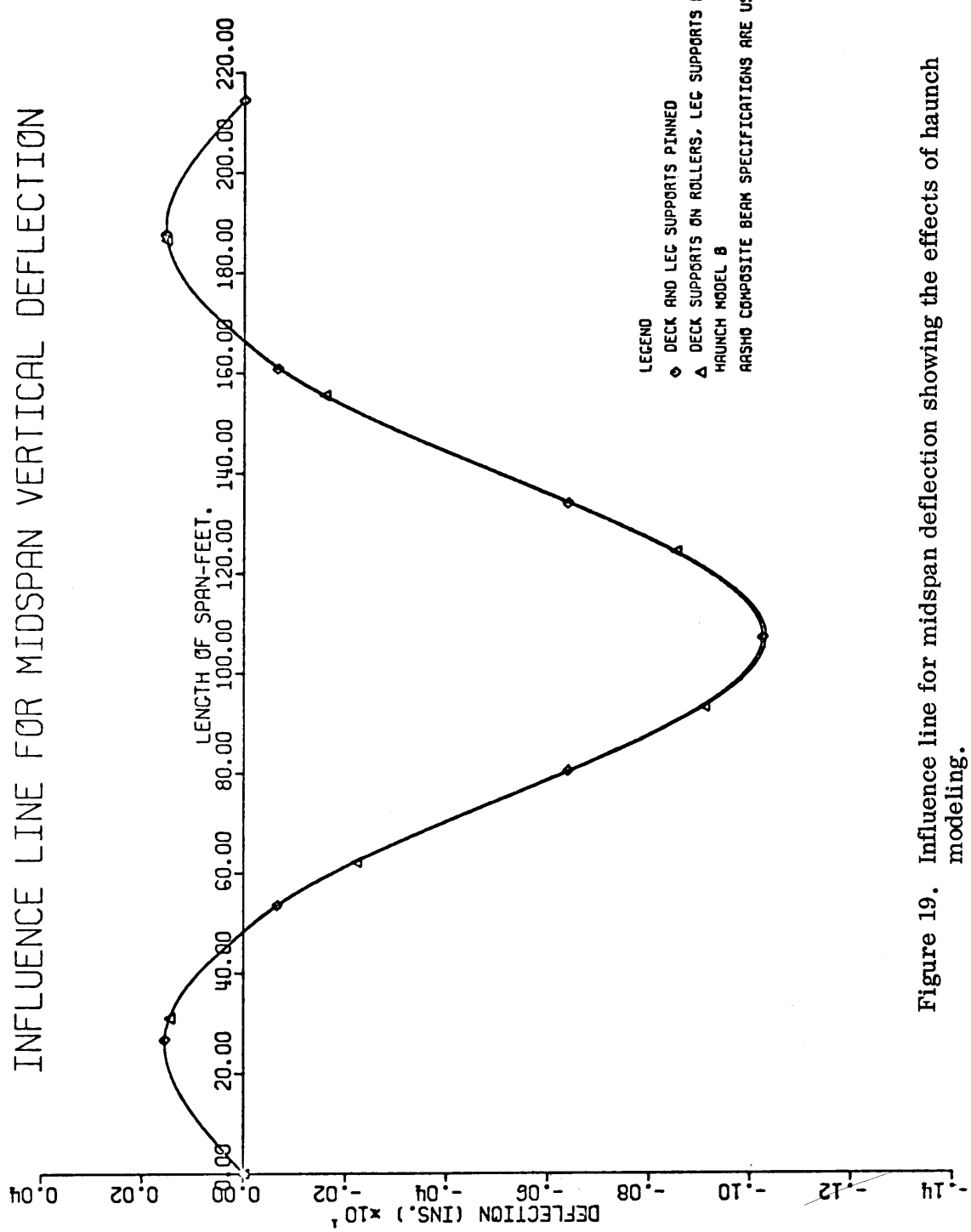

Figure 19. Influence line for midspan deflection showing the effects of haunch modeling.

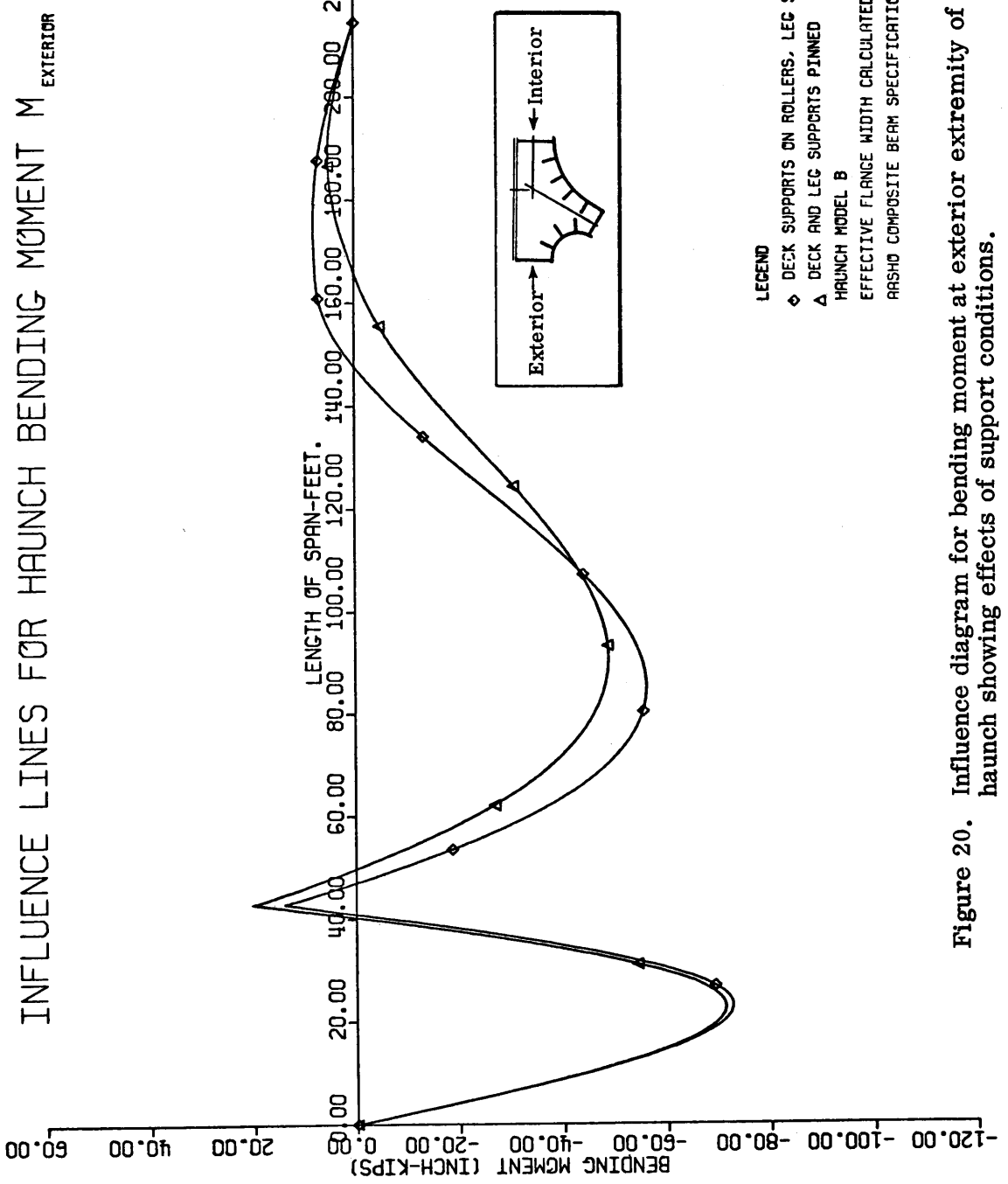

Figure 20. Influence diagram for bending moment at exterior extremity of haunch showing effects of support conditions.

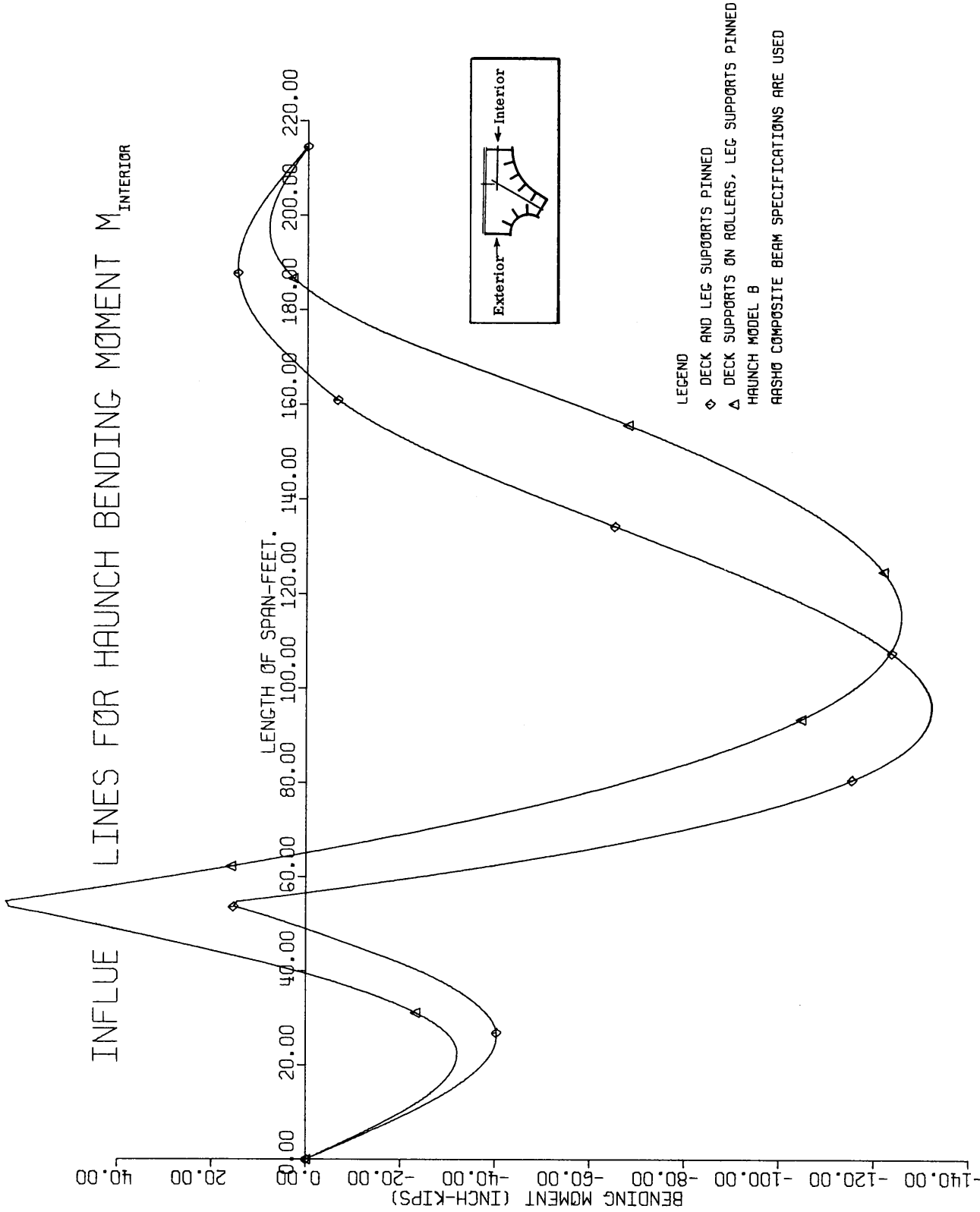

Figure 21. Influence diagram for bending moment at interior extremity of haunch showing effects of support conditions.

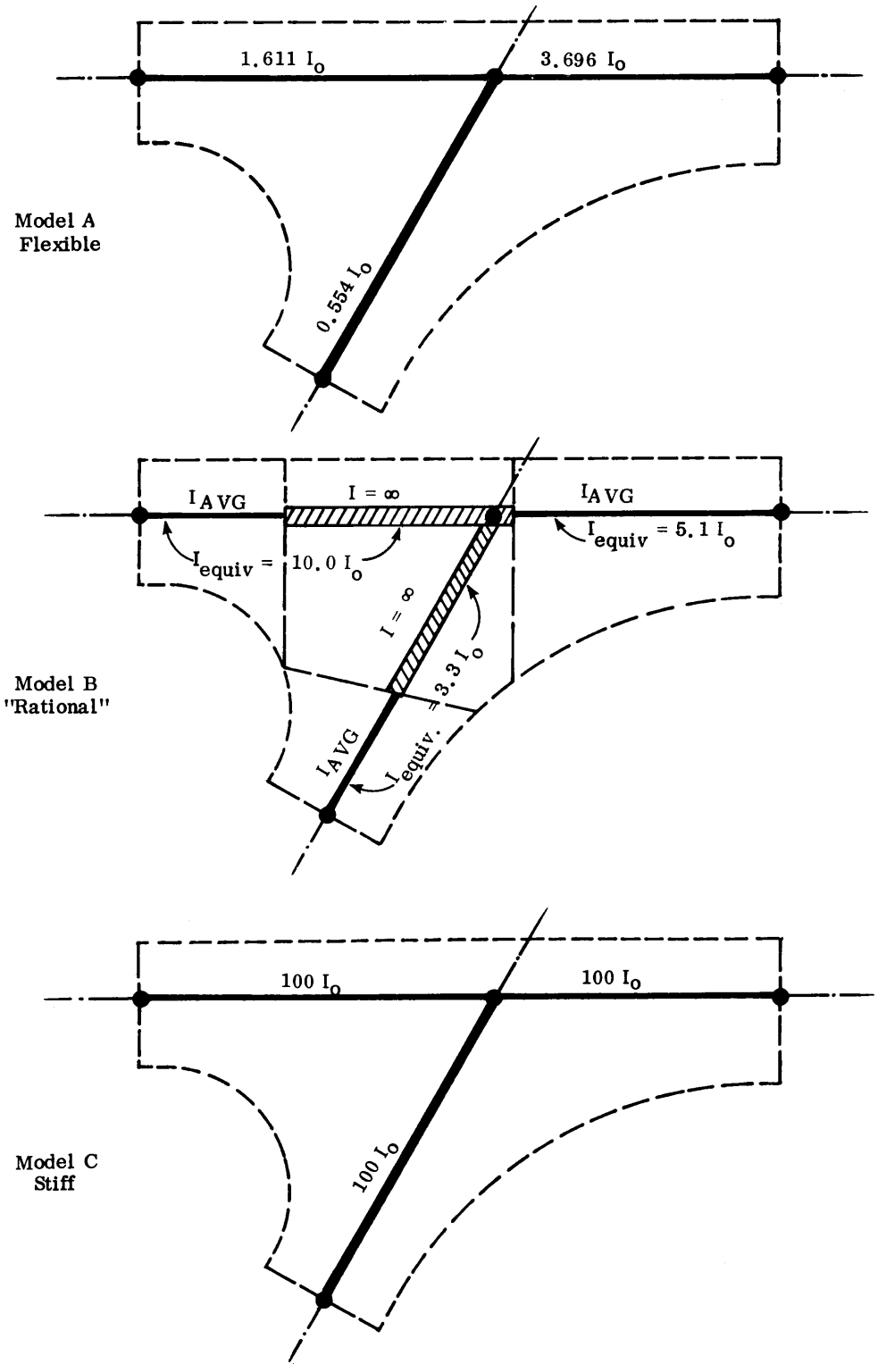

Figure 22. Sketches of various haunch idealizations.

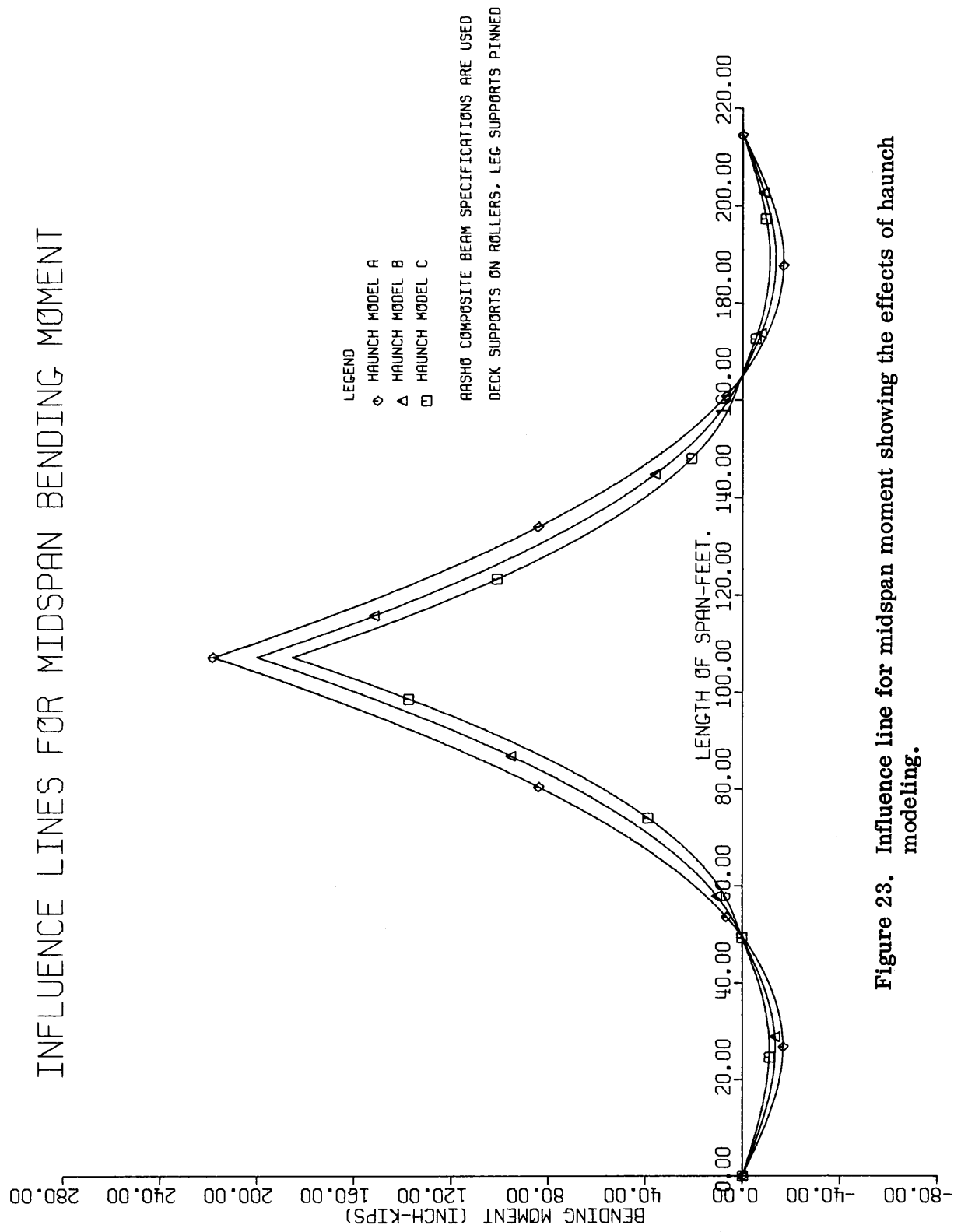

Figure 23. Influence line for midspan moment showing the effects of haunch modeling.

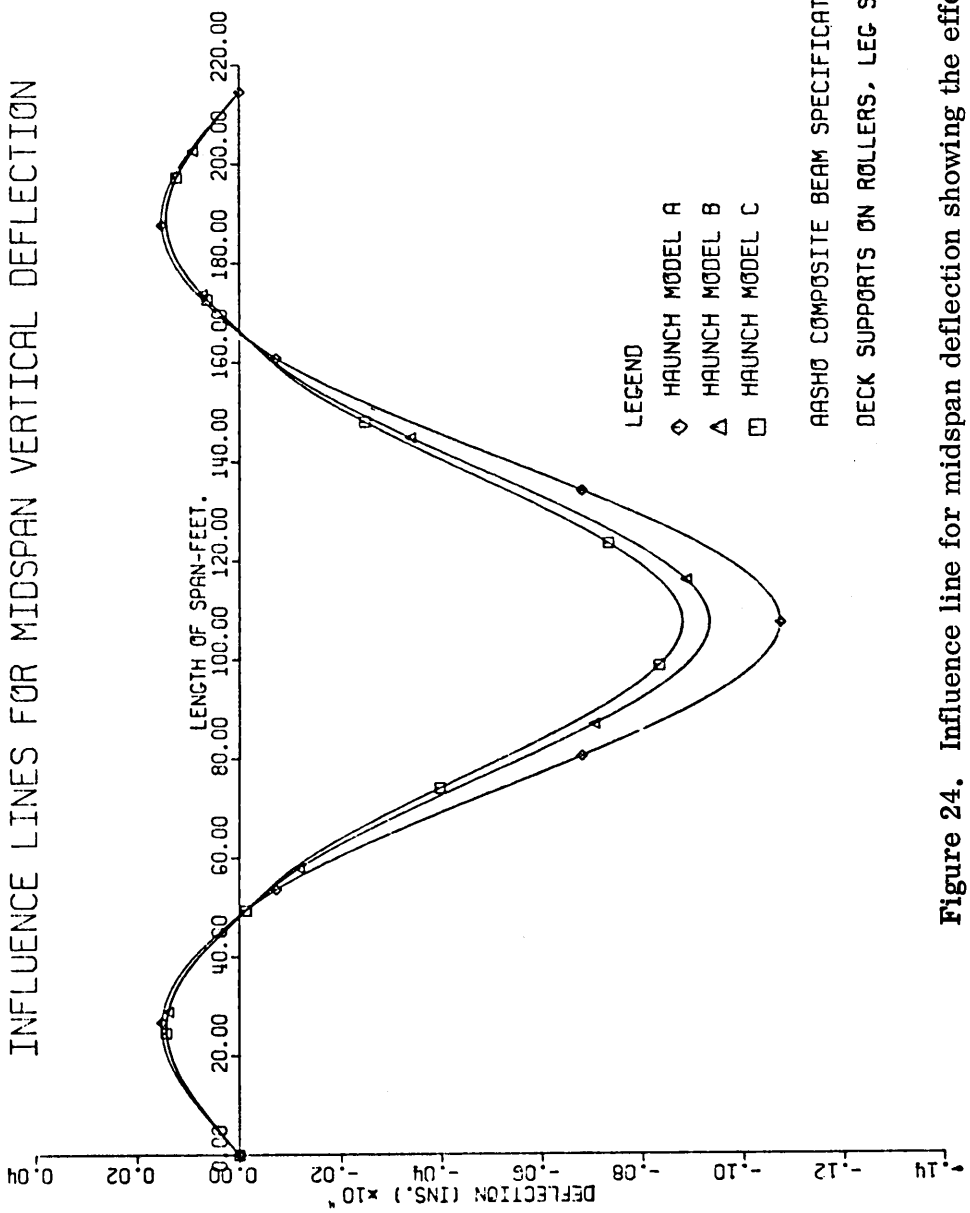

Figure 24. Influence line for midspan deflection showing the effect of haunch modeling.

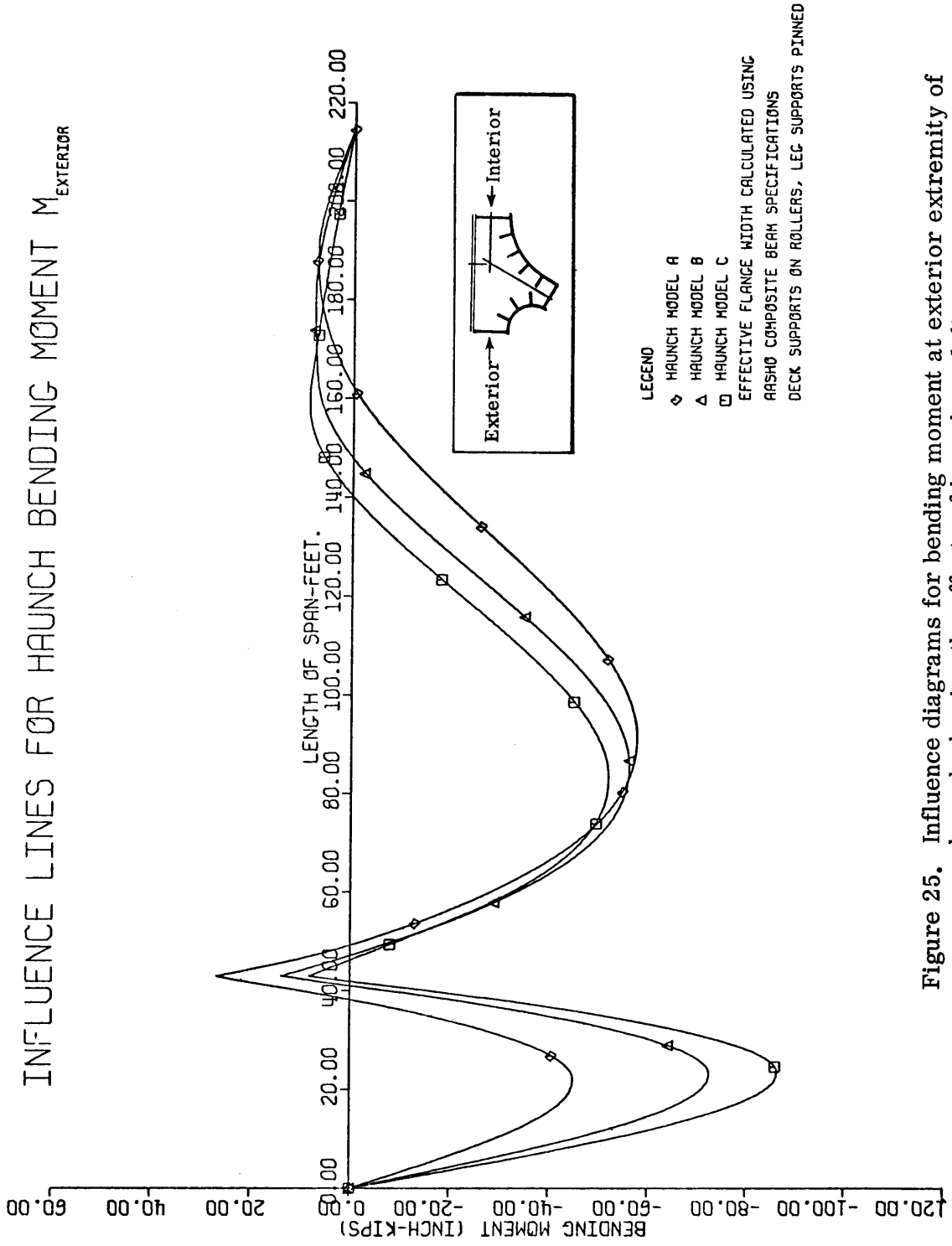

Figure 25. Influence diagrams for bending moment at exterior extremity of haunch showing the effects of haunch modeling.

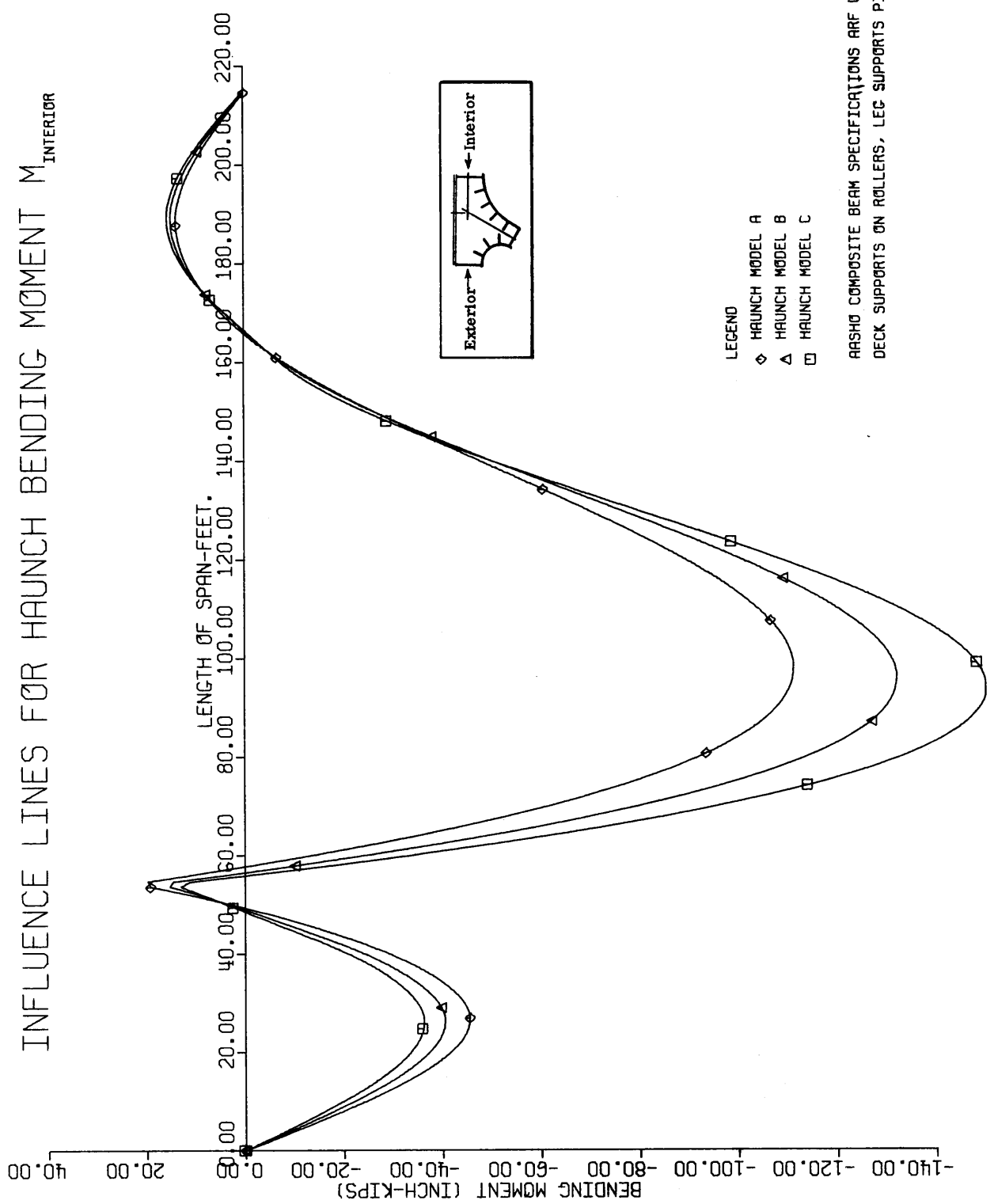

Figure 26. Influence diagram for bending moment at interior extremity of haunch showing the effects of haunch modeling.